PYROLYSIS OF CYCLOHEXANE AND BENZENE/CYCLOHEXANE MIXTURES IN A SINGLE PULSE SHOCK TUBE

by

B. Ellen Johnson

B.S., Kansas State University, 1981

MASTER'S THESIS

submitted in partial fulfillment of the
requirements for the degree

Master of Science

Department of Nuclear Engineering
KANSAS STATE UNIVERSITY
Manhattan, Kansas

1982

Approved by:

Thomas W. Lester
Major Professor

TABLE OF CONTENTS

LIST OF ILLUSTRATIONS

LIST OF TABLES

ACKNOWLEDGMENTS

I would like to thank the Department of Nuclear Engineering for their financial support, provided in the form of a graduate research assistantship. I also wish to thank the faculty and staff of the Department for their time and efforts spent on my behalf during my terms as a student of the Department.

To Dr. T. W. Lester and Dr. J. F. Merklin, I would like to express my sincere appreciation for their patience and encouragement during my undergraduate as well as graduate years. I am grateful for their guidance. A special thanks to Sharon Szydlowski for our innumerable discussions concerning this study and her technical assistance with the shock tube. I wish her the best in her future work. A special thanks, also, to Bob Stuewe, office-mate and friend, who provided much needed technical assistance with the electronic equipment.

Finally, I wish to thank my parents, because they never told me I couldn't do it.

1.0 INTRODUCTION

In recent years, much research has been focused on using our available fossil fuel resources efficiently. Although the economics of energy production are important, of equal importance are that the environmental consequences of the use of these resources be considered. Especially in the area of liquid petroleum fuels, the need to fit the pattern of availability to that of demand has resulted in a search for substitutes for these more preferable fuels. Additionally, there is a need to better use those fuels with less desirable characteristics and to develop combustors which can be easily tailored for fuels of varying qualities. Refining and upgrading of the lower quality, high boiling petroleum fuels is one possible solution, but this is not always economically viable. The introduction of liquids from coal and shale, while supplementing the amount of liquid hydrocarbons available as fuels, is hindered by the fuel specificity with which many combustors have been designed.

Several environmental and industrial problems arise from the use of these low quality fuel oils and coal liquids. Such fuels have physical characteristics which can result in less than optimum performance of various combustor systems.[1] For example, the high viscosity of the fuel may cause difficulties with the atomization and ignition of fuel droplets in a spray system. Chemically, the higher aromatic hydrocarbon content of these fuels, as compared to gasolines and middle distillates, results in lower thermal stability so that thermal stresses must be minimized and systems modified to maintain the fuel's integrity. The

many polyaromatic hydrocarbons (PAH) found in this energy source are also health hazards. Another major problem posed by the use of these aromatic fuels is that of an increased tendency to form soot. Soot, resulting from the incomplete combustion of the fuel, is an environmental as well as an industrial hazard. The aromaticity of the fuels may be decreased by hydrocracking, in which the hydrogen content is increased and the fuels are upgraded to the paraffinic range of distillates. However, such upgrading can become prohibitively expensive due to the need for a large and constant source of hydrogen.[2] Research pertaining to the use of fuels high in aromatic content has not only been concerned with possible changes in refining methods, but also with modifications of present combustors to compensate for the physical and chemical disadvantages of these aromatic fuels and their combustion products.

1.1 Objective of the Present Study

The current study concerns the pyrolysis of cyclohexane and benzene/cyclohexane mixtures in a single pulse shock tube. Observations of the product yield and distribution as a function of reaction temperature may lead to a more complete understanding of how aliphatic and aromatic constituents interact in the decomposition of alternative fuels. In both aliphatic and aromatic fuels, it has been observed that at least two types of hydrocarbons are active in the sooting process: acetylene and polyacetylenes, and polycyclic aromatic hydrocarbons (PAH). The thermal decomposition of the hydrocarbons in the absence of oxygen is the first step in determining the complex mechanism by which

soot is produced. In the modeling of hydrocarbon combustion and pollutant formation, the approach has increasingly been to model the subsets of the reaction mechanism, i.e., the H_2/O_2 and the CO/O_2 systems.[3] Such modeling often utilizes the quasi-global approach, in which the breakdown of the complex fuel constituents to simpler hydrocarbons, such as methane and acetylene, is modeled by an overall step. Little is known, however, about how the presence of both aromatic and aliphatic hydrocarbons affects the decomposition of each. Comparison of the cyclic aliphatic system, which can be viewed as a hydrogenated aromatic, to the aromatic system and the effect of one upon the other could suggest ways to decrease the tendency of the aromatics to soot.

1.2 The Formation of Soot

Soot is not well defined. Generally, it is considered to be made mostly of carbon, with traces of other elements, and up to 10 mole percent of hydrogen, the hydrogen content depending upon the age of the soot.[4] Soot first appears in the form of spherical carbon particles with an amorphous structure. These particles join to form aggregates and, as dehydrogenation occurs, the density of the aggregates increases. The crystalline structure of the carbon is like that of graphite, with layers oriented parallel to the particle surface or to centers within the particles. Once the aggregates form, the external layers extend from one particle to another so that individual particles lose their distinction.[5] The formation of soot during the combustion process is dependent on such factors as the fuel/air ratio, the chemical structure

of the fuel, and combustor operating conditions. Specifically, steady state operation of a combustor fueled with a stoichiometric paraffinic fuel/air mixture should not present sooting problems. However, if the combustor conditions are those of start-up or partial load, the fuel is highly aromatic, or the mixture fuel-rich, problems due to the production of soot may occur. Thus, the mechanism of soot formation must be examined so that combustors can be designed whose operation and maintenance are not adversely affected by the use of fuels high in soot-producing aromatics.

There are three basic steps in the sooting process: nucleation, condensation, and coagulation. Presently, there has yet to be a single model of the mechanism of soot formation to be generally accepted, and, indeed, there may not be any one mechanism. Theories put forth have included the condensation of carbon vapor into solid carbon, polymerization of the fuel, and production of solid carbon via acetylene.[6] Further discussion will be limited to the theory of acetylene as a soot precursor, as well as the more recent views on the importance of polyaromatic hydrocarbons in soot production. To add yet another dimension to an already complex problem, Palmer and Cullis,[7] in a review of the formation of carbon from gases, state that there is a distinction between carbon formed in the gas phase and that formed on a surface, and this difference must be taken into account when investigating carbonaceous solids. For the present study, however, it was assumed that carbon is produced only in the gas phase.

When pyrolyzed, most hydrocarbons decompose to acetylene in such quantities that it has been proposed as an intermediate in soot

production. Polymerization of the acetylene is one possible route to soot. Bradley and Kistiakowsky[8] found species which they identified as vinylacetylene and vinyldiacetylene during the pyrolysis of acetylene, and observed a decrease in the concentrations of these polyacetylenes corresponding to the beginning of carbon formation. Abrahamson[9] suggests that the precursors of soot, formed from acetylene, are large radicals which will react with acetylene to form particles in the form of platelets. These platelets have a hydrogen/carbon ratio near 1, and undergo dehydrogenation to form soot. If there is an aromatic present, radicals such as phenyl will add on acetylene to form the saturated platelet radicals. Eventually, the platelets may form a stable soot nucleus, or become PAH compounds. The view that PAH are by-products rather than intermediates in the production of soot is one that is being challenged by a number of studies, discussed below, which suggest that PAH are an indispensible part of the growth process leading to soot in both aliphatic and aromatic hydrocarbon systems.

A model of soot formation, accounting for the difference in sooting tendency between aliphatic and aromatic hydrocarbons, was proposed by Graham, et al.[10] and is shown in Fig. 1.1. Below 1800 K, the condensation of aromatic rings is favored, while above 1800 K, the fragmentation of the hydrocarbon and subsequent polymerization of the small fragments is the dominate pathway. Aliphatic hydrocarbons produce soot only by the second route, a slower process than the aromatic condensation. Study of soot formation from hydrocarbons has not filled the need for information on the interactions between aromatic and non-aromatic fuel constituents. Scully and Davies[11] investigated the

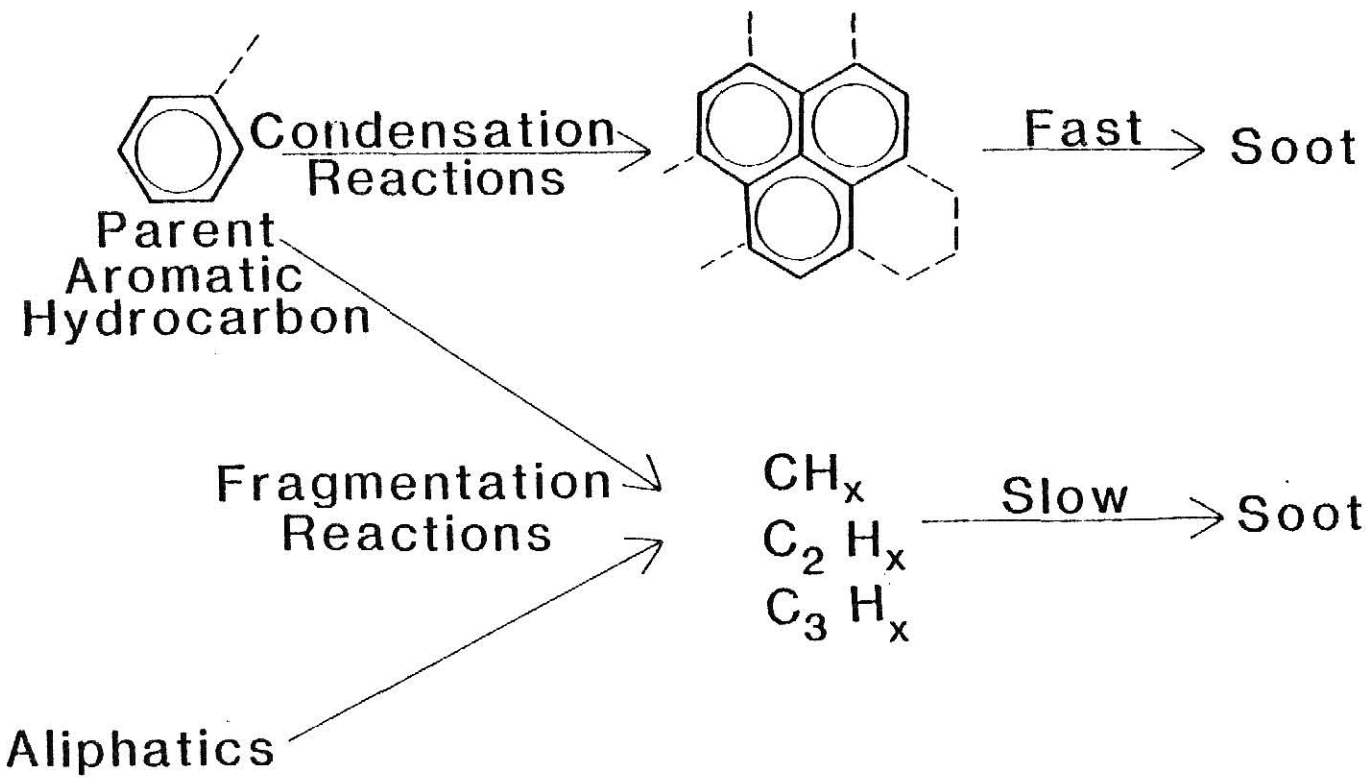

Fig. 1.1 Model of soot formation by Graham, et al.[10]

formation of carbon from benzene and cyclohexane injected into a town gas-air flame. It was found that cyclohexane did not produce a solid product, though a mist was observed in the exhaust, and only small yields of carbon black resulted from the decomposition of mixtures of 50% benzene/50% cyclohexane and 75% benzene/25% cyclohexane. The lack of sooting was explained, in part, as due to the increase in the amount of hydrogen in the cyclohexane system. An important observation was of a yellow-brown condensate indicating the presence of polycyclic aromatics, obtained from the carbon black produced by benzene. From these findings, it was concluded that ring rupture is not essential to the carbon forming process; rather, intact aromatic rings promote the formation of carbonaceous solids. This, of course, is also the conclusion of Graham, et al.

Bittner and Howard[12] have put forth a mechanism which proposes that the role of the aromatic in soot production is to provide a structure capable of stabilizing radicals formed by addition of non-aromatic hydrocarbons. Their probing of low pressure, pre-mixed, flat benzene/oxygen flames with a molecular beam mass spectrometer showed the high mass material produced to be aromatic rather than polyacetylenic in nature. They also conclude that the method of production of the polyaromatic hydrocarbons is influenced by the radical concentration. Lahaye and Prado[13] discuss studies which have shown that aromatics with side chains tend to produce more soot than those without side chains. Nelson,[14] using a shock tube to study benzene and toluene, reported toluene produced 20% more soot than benzene. This supports the findings

of Bittner and Howard in that toluene is the result of the addition of a methyl radical to a simple aromatic, which could be the first step in the production of PAH associated with soot.

Graham[15] investigated the nucleation and growth of soot from aromatics using a shock tube and has postulated that the nucleation step for soot formation is physical, rather than chemical, in nature. Chemically, the nucleation step is the chemical bonding of large molecules. Physically, the first step in the sooting process is the condensation of gaseous PAH into liquid droplets, with growth being accomplished by particle-particle collisions. The particles are part solid carbon and part liquid PAH, and have collisions which are perfectly coalescent. Lahaye and Prado[13] agree with the concept of the condensation of PAH as the nucleation step, but have an additional viewpoint concerning the manner of growth of the particles. They propose that surface growth of the particles involves the addition of gaseous macromolecules. [Prado[16] heated benzene to 110°C in a furnace and found a difference between the growth of particles during their formation and the growth of particles which are already formed.]

For polyaromatic hydrocarbons to be intermediates in soot formation, a supersaturated vapor of the PAH capable of condensing into droplets must be produced in some manner.[6] The formation of soot may be considered as a process beginning with PAH going to higher molecular weight products, and finally to soot. In support of the viewpoint that PAH are important in the sooting process is the fact that one of the products of the pyrolysis of hydrocarbons is tar. Tars are composed of PAH, some with aliphatic side chains. To determine if these tars, which

sometimes adsorb onto the surface of carbon particles, are intermediates or by-products of soot, Prado[16] observed that, during the pyrolysis of benzene, the tar yield reached a maximum when carbon black began to form, and then decreased. The conclusion that can be drawn is that PAH are intermediates, not by-products, of soot.

No matter if PAH are viewed as intermediates or as by-products in sooting, their presence is cause for concern because of the health hazards they represent if released from the combustion system. Poly-aromatic hydrocarbons have been identified as carcinogens and possible mutagens.[2] They are released either as gaseous products of combustion or as liquids adsorbed onto the soot particles, and can cause both air and water pollution. Because soot is in the particle size range which can enter the human respiratory system, the combined presence of soot and PAH becomes even more hazardous. This aspect of soot and its formation poses yet another problem which must be resolved before fuels with aromatic constituents will be accepted as alternatives to the paraffinic petroleum liquids.

1.3 The Thermal Decomposition of Cyclohexane

Cyclohexane is the alicyclic counterpart of benzene, the simplest of the aromatic hydrocarbons. Refining of a fuel with a high content of aromatics could include hydrogenation of the aromatics to alicyclics. Cyclohexane (C_6H_{12}) is a liquid under standard conditions, and is often used as an organic solvent. When comparing ring strain of cyclic compounds, cyclohexane is considered to be strain free, due to its

structure known as a chair conformation, and is the standard used for comparison.[17] It is also more thermally stable than hexane, a straight-chain hydrocarbon with the same number of carbon atoms.

The pyrolysis of cyclohexane has been studied at temperatures lower than those encountered in combustion. Its decomposition results in hydrogen, methane, ethylene, butadiene, and propene, and occurs according to a radical chain mechanism.[18,19] Thermal decomposition of cyclohexane in a tubular flow reactor also yields benzene, C_5 olefins, and acteylene.[20] From the studies of the decomposition of cyclohexane in a single pulse shock tube at reaction temperature of 970-1210 K, Tsang[21] proposed the mechanism shown in Fig. 1.2, where 1-hexene is formed from an initial cyclohexane decomposition step, and not from the degradation of a cyclohexyl radical. Another pathway described by Virk,[20] and shown in Fig. 1.3, does have a cyclohexyl radical decomposing to a hex-1-ene-6-yl radical, which can stabilize to 1-hexene.

Stein and Rabinovitch[22] studied unimolecular reactions of cycloalkyl radicals in the gas phase, and found that cyclohexyl radicals, unlike cyclic radicals of fewer carbon atoms, do not react to form straight chain ring-opened products, but produce methycyclopentyl radicals. The formation of the methylcyclopentyl radicals may be due to direct isomerization (by way of a transition state) or to a ring-opening, ring-closing process. The cyclohexyl to methycyclopentyl decomposition pathway is also supported by evidence from Tsang[23] and Satanova, et al.[24] This mechanism supports the observations of Scully

INITIATION

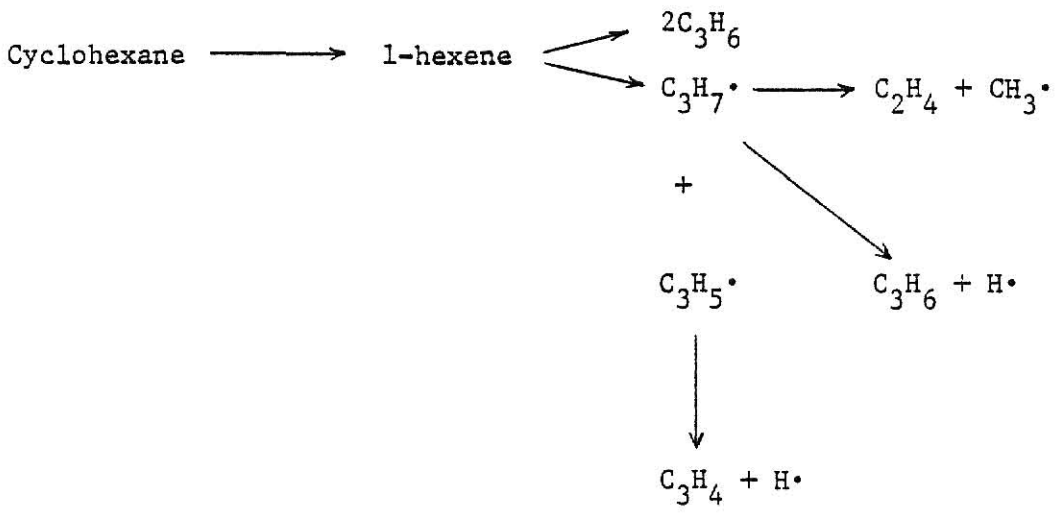

DECOMPOSITION OF CYCLOHEXYL (from R· + cyclohexane)

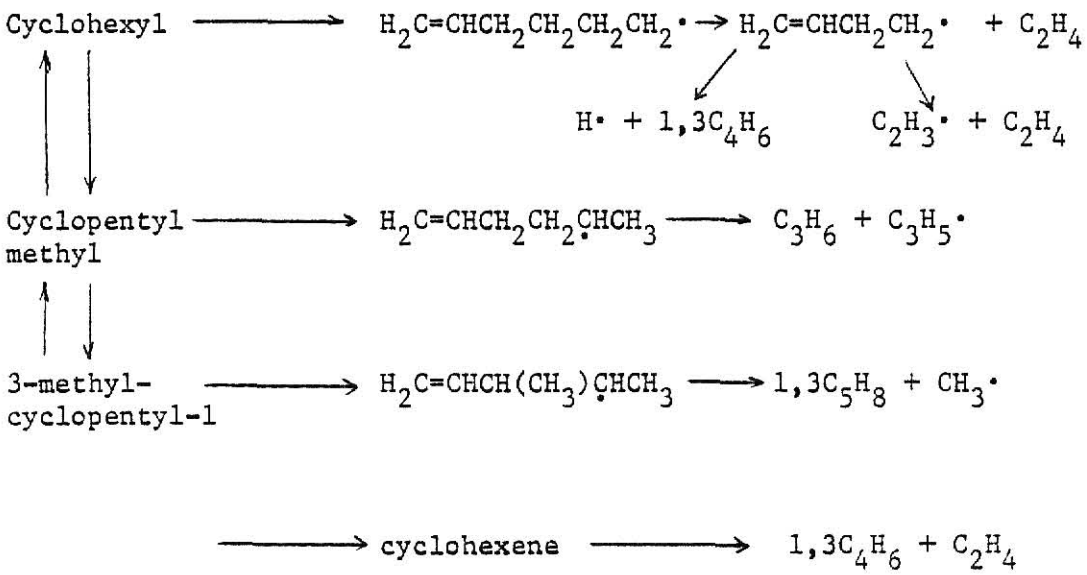

Fig. 1.2 Mechanism of the decomposition of cyclohexene as given by Tsang.[21]

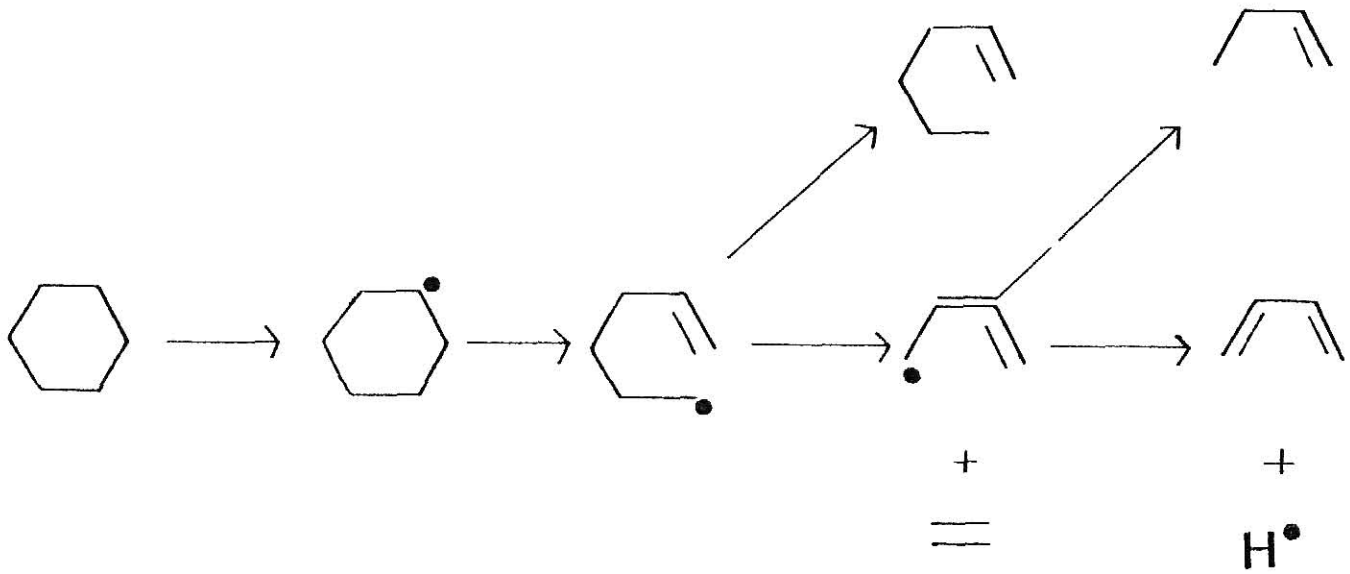

Fig. 1.3. Pyrolysis pathways for cyclohexane as reported by Virk, et al.[20]

and Davies[11] that cyclohexane produces less soot than benzene due to the destruction of its ring.

Investigation of the thermal decomposition of cyclohexane and mixtures of cyclohexane with an aromatic may lead to a clearer understanding of the roles of aliphatics and aromatics in soot production. Though benzene has been extensively studied at combustion temperatures, cyclohexane has not. It is possible that a single model for soot formation may not be possible if the two hydrocarbon systems act independently and along separate pathways in the sooting process.

2.0 EXPERIMENTAL PROCEDURE

2.1 The Single Pulse Shock Tube

The single pulse shock tube (SPST), as a reactor for studying the thermal decomposition of chemical systems, has certain advantages over other apparatus, such as flow reactors. The SPST allows for rapid heating, cooling, and pressurization of the reactants for a time period on the order of a millisecond, and the reaction zone is theoretically free of temperature, pressure, and velocity gradients. The SPST used in this study has been well characterized in a number of previous publications,[25-28] so that only a brief introduction to the apparatus will be presented.

In its simplest form, a shock tube consists of gas at high pressure, referred to as the driver gas, separated from a gas at a lower pressure by a diaphragm. Rupture of the diaphragm leads to compression waves in the low pressure gas which coalesce to form a planar shock front. There exists a change in temperature and pressure across the shock front, which, though finite, may be approximated as a step change. In addition to the shock front moving through the low pressure gas, a contact surface between the driver and low pressure gases follows the shock front while expansion waves propagate in an opposite direction into the driver gas. Figure 2.1 is a displacement-time diagram showing the progression of the shock front, contact surface, and rarefaction waves in a shock tube.

In gases, a sound wave moves through the medium by way of an isentropic process: collisions occur between molecules at a rate which is dependent on both the nature and state of the gas. Unlike a sound

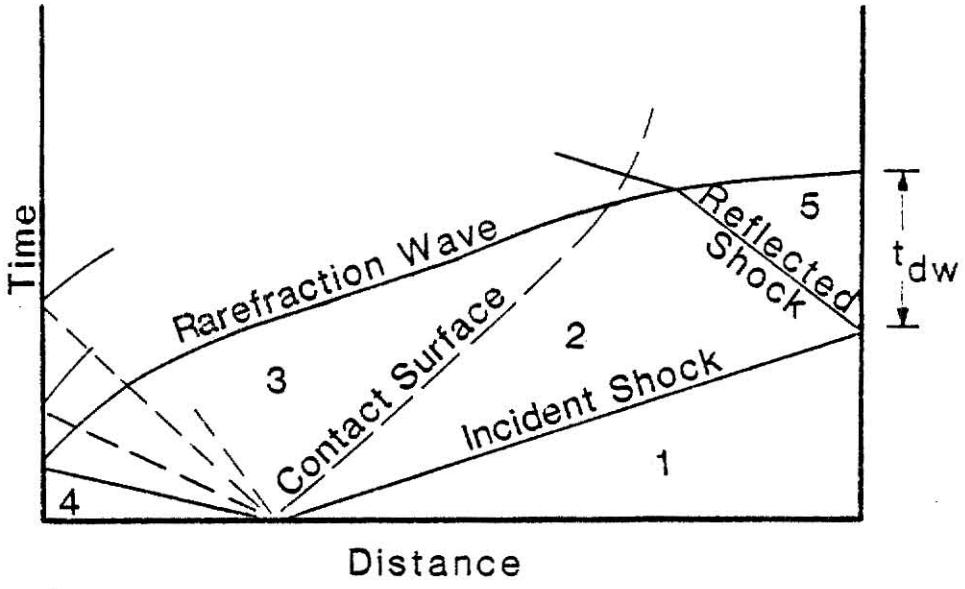

Fig. 2.1 A time versus distance diagram of the waves in a shock tube

wave, a shock wave, though adiabatic, is not isentropic. The strength of a shock wave can be described in terms of the speed of sound (a_1) in the gas, which in turn is temperature dependent.[30] Because a shock wave moves faster than the speed of sound for the gas in which it travels, there exists a flow in the direction of the front's movement. Changes in the physical states, such as pressure and temperature, across the shock front are caused by the collisional transfer of directed kinetic energy and the subsequent degradation of the energy into random kinetic energy.

To form a shock wave, there must be some way to form a supersonic wave series, such as rupturing a diaphragm between high and low pressure gases. The resulting compression waves which propagate into the low pressure gas will each have a speed greater than the preceding wave as it passes through the gas heated by that previous wave. Though the compression waves will not overtake one another, they will join together to form a planar shock front. The shock front moves with a velocity (V_1) corresponding to a Mach number of

$$M_1 = \frac{V_1}{a_1} \tag{2.1}$$

into the low pressure static gas while the gas behind the front is moving at a slower velocity. The incident shock wave reflects from the end wall of the shock tube and propagates into the oncoming gas. Since a shock wave always accelerates the gas through which it travels in the direction of its propagation, the oncoming gas is suddenly decelerated. In the limit of perfect reflection, the velocity of gas behind the reflected shock becomes zero. By using the conservation equations and

assuming the gas velocity behind the reflected shock wave is zero, and the gas is both thermally ($P=\rho RT$) and calorically (c_p/c_v=constant) perfect, i.e. ideal, the temperature and pressure of the gas behind the reflected shock may be calculated by [29]

$$T_5 = T_1 \left\{\frac{[2(\gamma-1)M_1^2 + (3-\gamma)][(3\gamma-1)M_1^2 - 2(\gamma-1)]}{(\gamma+1)^2 M_1^2}\right\} \qquad (2.2)$$

and

$$P_5 = P_1 \left\{\frac{2\gamma M_1^2 - (\gamma-1)}{\gamma+1}\right\} \left\{\frac{(3\gamma-1)M_1^2 - 2(\gamma-1)}{(\gamma-1)M_1^2 + 2}\right\} \qquad (2.3)$$

where

γ = specific heat ratio of the gas,
M_1 = Mach number of the incident shock wave,
T_1 = initial temperature of the low pressure gas, and
P_1 = initial pressure of the low pressure gas.

Cooling occurs when the reflected rarefaction fan overtakes the contact surface and continues to propagate into the stagnant, heated gas behind the reflected shock wave. The cooling rate is finite and much slower than the heating rate of the gases. When the contact surface is allowed to interact with the reflected shock wave, it will either come to rest or will cause mixing of the gases along with further shock and rarefaction waves. The useful reaction time behind the reflected shock front is limited by the arrival of the rarefaction fan at the reaction zone near the end wall of the tube. This time at conditions of T_5 and P_5 is the dwell time (t_{dw}), and is defined as the period of time between the passage of the reflected shock and the arrival of the rarefaction fan at a given location (see Fig. 2.1). This dwell time, however, must be corrected; although the cooling rate is greater than -10^5 K/sec, not all reactions are quenched effectively. For reactions with a low

activation energy (E_a < 60 kcal/mole), the thermal decomposition which occurs during the cooling must be taken into account. The correction for the finite cooling rate, as proposed by Tschuikow-Roux[31] is discussed in Appendix A.

The single pulse shock tube facility at Kansas State University was originally designed and built by Seeker.[25] The SPST differs from a conventional shock tube in that the experimental gas is heated by only one reflected shock wave. The wave is prevented from repeatedly reflecting off the end walls of the tube by the addition of a dump tank set at an oblique angle into the tube, as seen in Fig. 2.2. The reflected shock front will preferentially travel into the dump tank, which remains at the initially low pressure as the front travels down the tube.

The tube is made of type 304 stainless steel with an inner diameter of 5.08 cm and a tube thickness of 0.635 cm. The tube is divided into several sections to provide the ability to change the length, the maximum length being 10 meters, as dictated by the desired experimental conditions. For the present study, the driver section was varied from 1 to 2 meters in length. The low pressure section was 5 m long, and the experimental section was attached to it by means of an in-line ball valve. The test, or experimental section, as described by Szydlowski[28] and shown in Fig. 2.3, is 29.5 cm in length and has an inner diameter of 5.7 cm. The slightly larger diameter allows for the insertion of removable aluminum liners which may be used for solid and liquid recovery. The aluminum liners have the same inner diameter as the remainder of the tube. In-line filters of activated charcoal and molecular sieve 5A have been installed to absorb moisture and

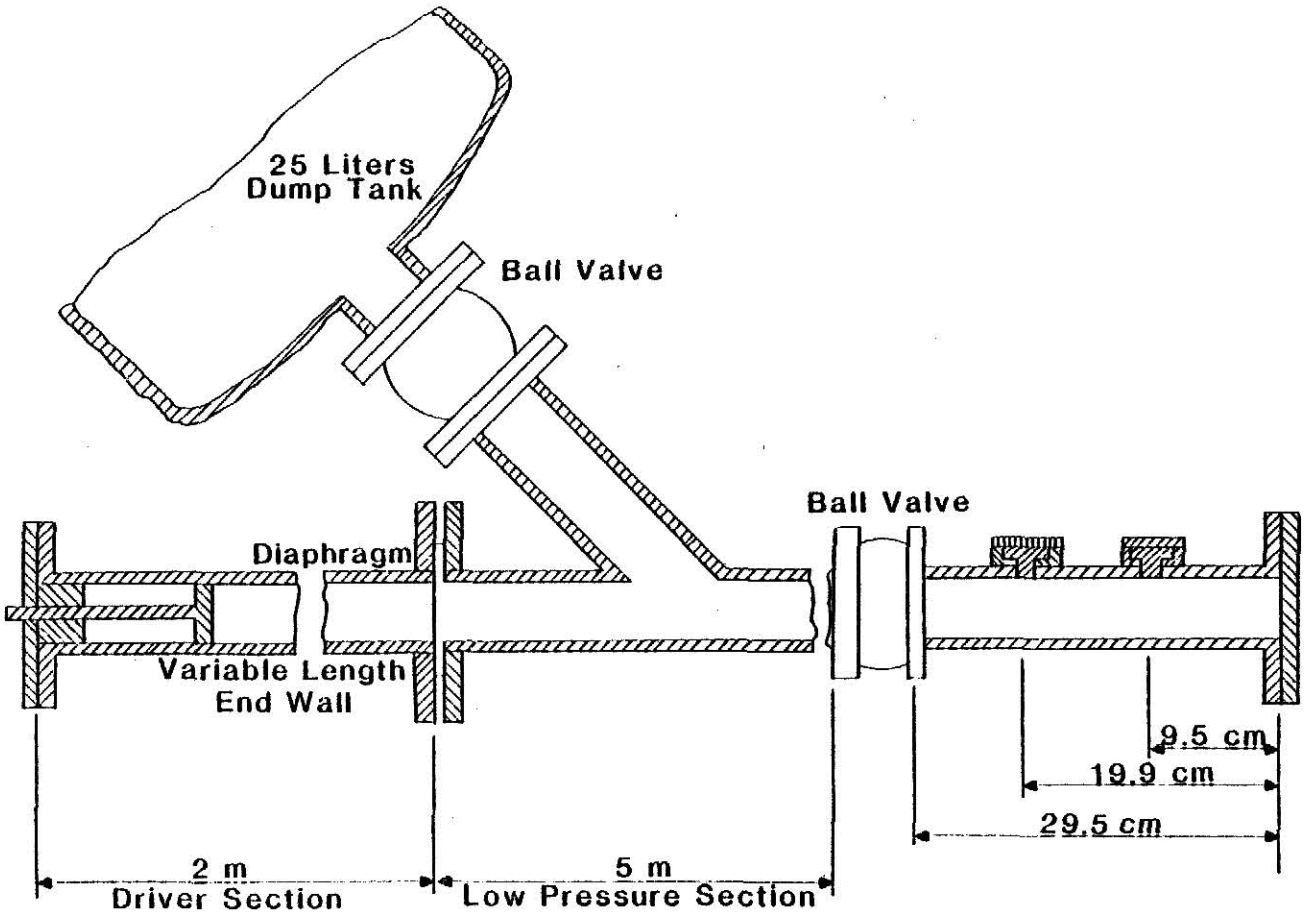

Fig. 2.2 Schematic of the single pulse shock tube

hydrocarbons from the gases, thus minimizing contamination of the tube. Helium (99.99% purity) was used as a driver gas rather than hydrogen because, while it has a high speed of sound, it is not explosive. The low pressure section was filled with argon (99.995% purity) to provide a nearly inert atmosphere for the reaction and a closer approximation to an ideal gas system. The experimental section contained the reactant/gas mixture to be studied. The driver section was evacuated to less than 1 Torr of pressure using a Duo Seal vacuum pump (Model 1402). The low pressure and experimental sections were evacuated to a pressure of less than 50 mTorr with a Duo Seal vacuum pump (Model 1405) and then further evacuated to less than 1 mTorr by a Veeco two-inch water cooled oil diffusion pump. The diaphragm, used to separate the driver and low pressure sections, was made of 0.4 mm thick aluminum. As suggested by Gaydon and Hurle,[29] the diaphragm was scribed at right angles so that, upon rupture, the metal petalled back to allow passage of the driver gas. The diaphragm was mechanically burst by means of a pointed plunger set at an angle into the driver section.

The experimental gas mixtures, composed of the desired reactants diluted with argon, were produced by injecting a known amount of reactant into an evacuated 500 cm^3 stainless steel container and pressurizing the bottle to 6.87 X 10^5 Pa with the diluent. The reactants studied were cyclohexane (99 mol% pure, Fisher Scientific Company), benzene (99 mol% pure, thiophene free, Fisher Scientific Company), and benzene/cyclohexane mixtures, and were referred to as stock mixtures. To begin an experiment, or run, clean aluminum liners were placed in the test section, and the tube was evacuated. After evacuation of the low pressure and test sections, the in-line ball valve

was closed and the stock mixture introduced into the test section, by means of the system shown in Fig. 2.3, to 120-440 Torr. The low pressure section was filled to the same pressure (P_1) with argon. The driver section was then pressurized to 18-20 x 10^5 Pa with helium. The in-line ball valve was opened, the diaphragm punctured, and the shock wave initiated. The in-line ball valve was manually closed immediately after the run to trap the product gases in the experimental portion of the tube. The final equilibrium pressure of the tube (P_e) was 1.5-3.0 x 10^5 Pa. The pressure ratio between the low pressure and driver sections was varied to yield shocks of different strengths.

The speed of the incident shock wave and the pressure history of the gas in the test section were recorded using two piezoelectric pressure transducers (Kistler, Model 603A) mounted in the test section as shown in Fig. 2.3. One transducer was placed 20 cm from the end wall, flush to the tube wall, and the second was mounted into the end wall. Output from each transducer was fed through a charge amplifier (Kistler, Models 504A and 504E) and a linear amplifier (Ortec, Model 410) into a digital counter (Fluke, Model 1925B). Input from the second transducer stopped the counter. Because the shock speed was used to determine the reaction temperature and pressure (Eqs. 2.2 and 2.3), experiments were conducted to confirm the accuracy of the temperature prediction. These experiments, which concerned the pyrolysis of n-butane, resulted in the judgement that the reaction temperature and pressure, as calculated from the shock speed, did not need correction. Further details are provided in Appendix B. Output of the pressure transducer mounted in the end wall also yielded a pressure history of the gas in the test section. A signal from the passage of the shock

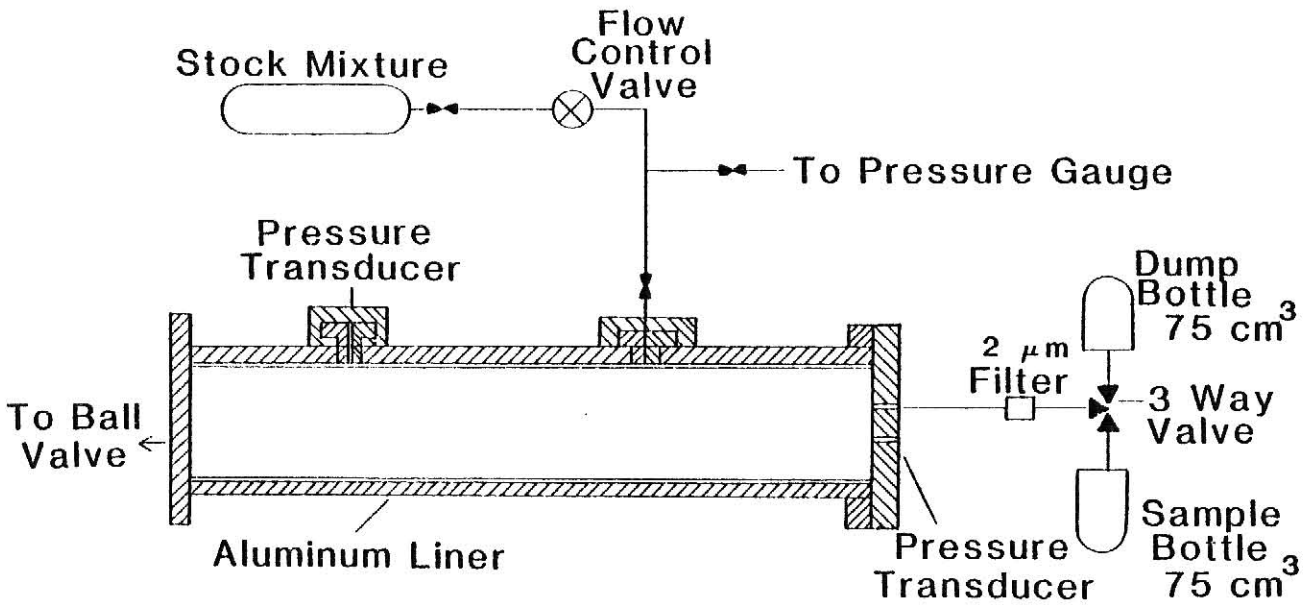

Fig. 2.3 Schematic of experimental section with gas delivery and sampling systems.

front past the first transducer triggered a storage oscilloscope (Tektronix Type 7623A), and output from the end wall transducer was displayed on the oscilloscope. The resulting oscillogram, an example of which is shown in Fig. 2.4, allowed estimation of the dwell time and conservation of any discontinuities in the system.

For experiments with a dwell time of 1.0-1.5 msec, designated as "non-soot runs", samples were taken after of one hour to provide time for the gases in the experimental section to diffuse and reach an equilibrium concentration.[32] As seen in Fig. 2.3, the product gases were first allowed to expand into a dump bottle to rid the sampling line of any unreacted stock mixture which may have remained in the line or filter. The gas sample used for analysis was then introduced into an evacuated 75 cm^3 stainless steel bottle. Shocks for which solid and liquid gravimetric analyses were performed have been designated as "soot runs." For these, the driver section was lengthened to yield a dwell time of approximately 2.5 msec. The longer dwell time allowed for the production of a measurable quantity of liquid and solid products. Sampling was delayed until 7-12 hours after the passage of the shock wave through the test gas to allow solids and liquids to deposit on the aluminum liners. After the gas sample was taken, the experimental section was allowed to come to atmospheric pressure by slowly venting the remaining gases. The liners were then removed for analysis. After each experiment, to prevent contamination of the tube from carryover of the reactants and products from one run to another, the test section, with the liners removed, was cleaned with acetone. A high temperature shock (T_5 > 2500 K) into 21.5% oxygen in argon was initiated. This process is referred to as the oxidation shock.

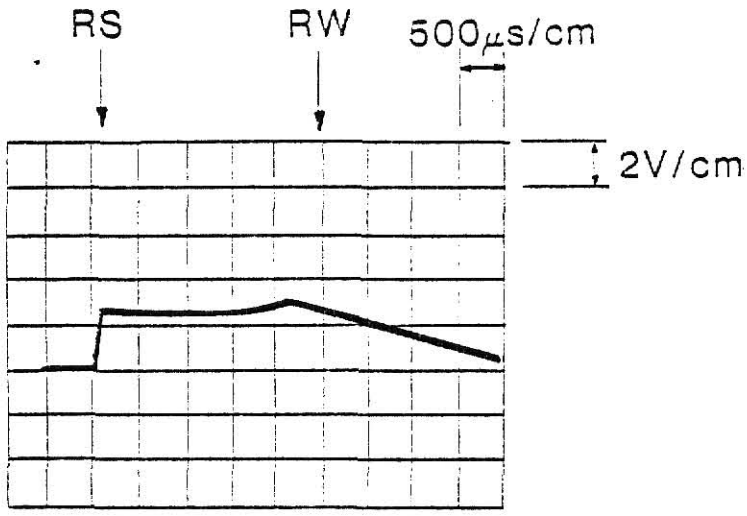

Fig. 2.4 Example of oscillogram of pressure history of gases in experimental section

2.2 Sample Analysis

2.2.1 Gas Analysis

Analysis of the gaseous samples was conducted with a Tracor Model 560 gas chromatograph equipped with dual flame ionization detectors. The minimum detectable level is approximately 1×10^{-9} g. Operating conditions for the columns are listed in Table 2.1. The SP2250 and Carbosieve B columns allowed for the detection of methane, ethylene, acetylene, cyclohexane, and benzene. Because of the low oven temperature, and subsequent length of time needed for analysis, the column for analysis of C_3 and C_4 hydrocarbons was only used for a specified set of shocks with cyclohexane as the reactant. The gas chromatograph was calibrated for each series of sample injections with predetermined volume of a known standard. For the present study, the injection volume was 200 μliters and the standard was acetylene (1030 ppm, Can Mix 232, Scott Specialty Gases). From analysis of a chromatogram, the mole percent of species i could be calculated by

$$m_i = \frac{W_a A_i F_a}{MW_i F_i A_a m_g}, \qquad (2.4)$$

where

m_i = moles of species i per mole of gas in sample injection,
W_a = weight of standard injected in grams,
A_a = peak area of standard,
A_i = peak area of species i
F_a = response factor for standard as reported by Dietz,[33]
F_i = response factor for species i,
MW_i = molecular weight of species i in grams, and
m_g = moles of gas per injection.

The yield of each product was calculated from

Table 2.1 Gas chromatograph operating conditions.

Column	Hydrocarbons analyzed	Oven Temperature (C)	Flow (cm^3/min)
10% SP2250 on 100/120 Supelcoport	$C_1 - C_7$	120	35
100/120 Carbosieve B	$C_1 - C_3$	200	45
0.19% Picric acid on 80/100 Carbopack C	C_3 and C_4	50	45

$$y_i = \frac{m_i P_e}{m_0 P_1} \qquad (2.5)$$

where

y_i = moles of species i yielded per mole of reactant pyrolyzed,
m_i = mole percent of species i in sample,
m_0 = mole percent of reactant in stock mixture,
P_e = equilibrium pressure in shock tube after experiment, and
P_1 = initial pressure in experimental section before passage of front.

2.2.2 Solid and Liquid Gravimetric Analysis

Gravimetric analysis of the solid and liquid residue on the aluminum liners was recorded for experiments designated as soot runs. Before initial evacuation of the experimental section, the liners were cleaned with acetone, heated for 1 hour at 400 K, cooled in a dessicator, and placed under a vacuum. This procedure was carried out to minimize weight gain due to atmospheric moisture or carryover of pyrolysis products remaining on the liners from previous runs. The liners were weighed using a Mettler H80 balance, and put into the test section. They were then weighed again after their removal from the test section 7-12 hours after the experiment was run. The gain in weight by the liners, giving a weight percent yield for solid and liquid products, was compared to the total weight of reactant present in the test section prior to the passage of the shock wave. Comments on the visual appearance of the residue were made when appropriate. Attempts to remove samples of the residue from the liners were not successful, and thus qualitative analysis of the residue was prevented.

3.0 RESULTS

A baseline investigation of the pyrolysis of cyclohexane was performed, as well as additional studies of the pyrolysis of benzene and benzene/cyclohexane mixtures, to determine the influence of the thermal decomposition of alicyclic and aromatic hydrocarbon systems on one another. The experiments were carried out at reaction conditions of 1400-2400 K and 7-13 X 10^5 Pa. Data concerning the gaseous products and gravimetric analysis of the solid and liquid residue are presented.

3.1 Gaseous Products

3.1.1 Cyclohexane

Data from the analysis of gaseous products of pyrolysis of cyclohexane are recorded in Table 3.1 and 3.2. To supplement the non-soot and soot runs, as defined in Section 2.1, experiments were conducted for which the dwell time was approximately 1.0-1.5 msec, and gaseous as well as solid and liquid gravimetric sampling was conducted after 7-12 hours. This additional set of runs was to aid in determining if the delay in sampling affected the gaseous product yields. Reactant mixtures of three concentrations were studied for the non-soot runs: 1.3 mol%, 0.8 mol%, and 0.4 mol% of cyclohexane in argon. Soot runs were carried out only with the mixture of the highest concentration.

Figures 3.1 and 3.2 are plots of the cyclohexane remaining in the sample after pyrolysis as a function of reaction temperature. The principal gaseous products were methane, ethylene, and acetylene. Yields are shown as a function of temperature in Figs. 3.3-3.6. While the yields of acetylene steadily increase with temperature for the

Table 3.1 Results of analysis of gaseous products from pyrolysis of cyclohexane

T_5 (K)	P_5 ($\times 10^5$Pa)	t_{dw} (msec)	$[C_6H_{12}]_0$	$\frac{[C_6H_{12}]T_{dw}}{[C_6H_{12}]_0}$	Product Yield (mole of product/mole of C_6H_{12})		
					CH_4	C_2H_4	C_2H_2
1444	11.9	1.2	0.0132	0.198	0.0474	0.271	0.0380
1461	10.7	1.0	0.0132	0.317	0.113	0.631	0.106
1525	11.5	1.2	0.0132	0.141	0.0665	0.459	0.0943
1589	11.4	1.2	0.0132	0.161	0.213	1.045	0.309
1660	10.5	1.1	0.0132	0.0363	0.290	1.180	0.478
1867	9.9	0.7	0.0132	0.0535	0.449	1.256	0.953
1886	10.5	0.8	0.0132	0.0487	0.429	0.783	0.931
1979	10.1	1.0	0.0132	0.0497	0.291	0.482	0.702
2048	10.1	1.4	0.0132	0.0311	0.288	0.306	0.852
2093	10.4	1.3	0.0132	0.0326	0.495	0.441	1.421
2110	9.3	0.8	0.0132	0.0393	0.439	1.390	1.480
2187	9.7	1.4	0.0132	0.0187	0.269	0.188	1.195
2228	9.3	1.3	0.0132	0.0318	0.426	0.233	2.083
2279	9.5	0.9	0.0132	0.0303	0.410	0.214	1.864
2287	8.3	0.9	0.0132	0.0194	0.272	0.122	1.280
2298	9.7	1.4	0.0132	0.0203	0.345	0.181	1.363
2314	9.1	1.4	0.0132	0.0336	0.315	0.128	1.508
1438*	11.1	1.2	0.0132	0.143	0.0472	0.234	0.0335
1481*	10.9	1.1	0.0132	0.181	0.123	0.632	0.116
1604*	11.5	1.2	0.0132	0.0466	0.122	0.445	0.154
1764*	10.4	0.7	0.0132	0.104	0.333	1.179	0.652
1881*	10.5	1.0	0.0132	0.168	0.415	0.862	0.821
1926*	9.7	0.7	0.0132	0.0292	0.454	0.989	1.215
1997*	10.2	1.3	0.0132	0.0334	0.450	0.715	1.163
2082*	9.7	0.8	0.0132	0.0519	0.415	0.383	1.325
2166*	10.2	1.5	0.0132	0.0414	0.435	0.269	1.697
1463*	7.9	2.0	0.0132	0.0769	0.0778	0.230	0.102
1685*	9.8	2.2	0.0132	0.0413	0.218	0.614	0.443

T_5 (K)	P_5 ($x10^5$Pa)	t_{dw} (msec)	$[C_6H_{12}]_0$	$\frac{[C_6H_{12}]T_{dw}}{[C_6H_{12}]_0}$	Product Yield (mole of product/mole of C_6H_{12}) CH_4	C_2H_4	C_2H_2
1558*	10.3	2.4	0.0132	0.0501	0.195	0.435	0.175
1721*	12.4	2.7	0.0132	0.0208	0.272	0.497	0.363
1756*	11.3	2.7	0.0132	0.0274	0.230	0.595	0.676
1817*	9.9	2.3	0.0132	0.0234	0.197	0.328	0.449
1852*	10.2	2.5	0.0132	0.0395	0.251	0.311	0.482
1970*	11.2	2.7	0.0132	0.0145	0.336	0.210	0.947
1985*	10.1	2.4	0.0132	0.0154	0.296	0.138	0.345
2249*	9.4	2.3	0.0132	0.0215	0.118	0.0650	0.623
2376*	8.7	2.3	0.0132	0.0205	0.0711	0.0233	0.303
1476	12.7	1.9	0.00793	0.133	0.110	0.450	0.123
1502	12.7	1.4	0.00793	0.107	0.0824	0.520	0.109
1698	11.7	1.5	0.00793	0.0242	0.241	0.643	0.447
1809	11.3	1.7	0.00793	0.0179	0.321	0.471	0.814
2036	10.5	1.3	0.00793	0.0742	0.361	0.604	0.945
2085	9.7	1.1	0.00793	0.124	0.250	0.043	0.886
2197	9.1	0.5	0.00793	0.0402	0.200	0.0183	0.681
1519	12.9	1.3	0.00396	0.575	1.558	5.588	2.485
1608	12.4	1.4	0.00396	0.267	2.489	6.355	4.742
1730	12.0	0.7	0.00396	0.239	3.477	3.944	8.228
1915	10.2	1.2	0.00396	0.218	3.165	0.978	7.897
2270	10.9	1.1	0.00396	0.169	0.865		6.957

*Soot run.

Table 3.2. Yields of C^3 and C^4 products from the pyrolysis of cyclohexane

T_5 (K)	P_5 ($\times 10^5$Pa)	t_{dw} (msec)	$[C_6H_{12}]_0$	$\frac{[C_6H_{12}]T_{dw}}{[C_6H_{12}]_0}$	Product yield (moles of product/mole of C_6H_{12}) propene and propyne	1,3 butadiene	1,2 butadiene
1424	11.7	1.2	0.0132	0.244	0.035	0.111	0.00521
1483	12.8	1.5	0.0132	0.193	0.0418	0.137	0.00602
1599	13.1	1.8	0.0132	0.0976	0.0592	0.118	0.0101
1642	12.0	1.5	0.0132	0.0674	0.0660	0.119	0.0111
1672	9.7	1.0	0.0132	0.0456	0.0694	0.102	0.0155
1689	10.7	1.5	0.0132	0.0272	0.0729	0.0820	0.0131
1689	11.7	1.6	0.0132	0.0360	0.0784	0.0981	0.0162
1842	11.2	1.9	0.0132	0.0215	0.0714	0.0538	0.0236
1912	10.7	1.1	0.0132	0.0141	0.0340	0.0290	0.0178
2033	9.3	0.9	0.0132	0.0230	0.0301	0.0173	0.0111
2150	9.5	1.0	0.0132	0.0315	0.0255	0.0197	0.00910
2311	9.8	1.5	0.0132	0.0217	---	0.0149	---
1694*	11.6	2.6	0.0132	0.0393	0.0575	0.0595	0.0183
1982*	10.7	2.5	0.0132	0.0138	0.0304	0.0292	0.0113
2121*	8.7	2.3	0.0132	0.0149	0.0160	0.0489	---
2140*	9.4	2.3	0.0132	0.0235	0.0214	0.0135	0.00643

*Soot run.

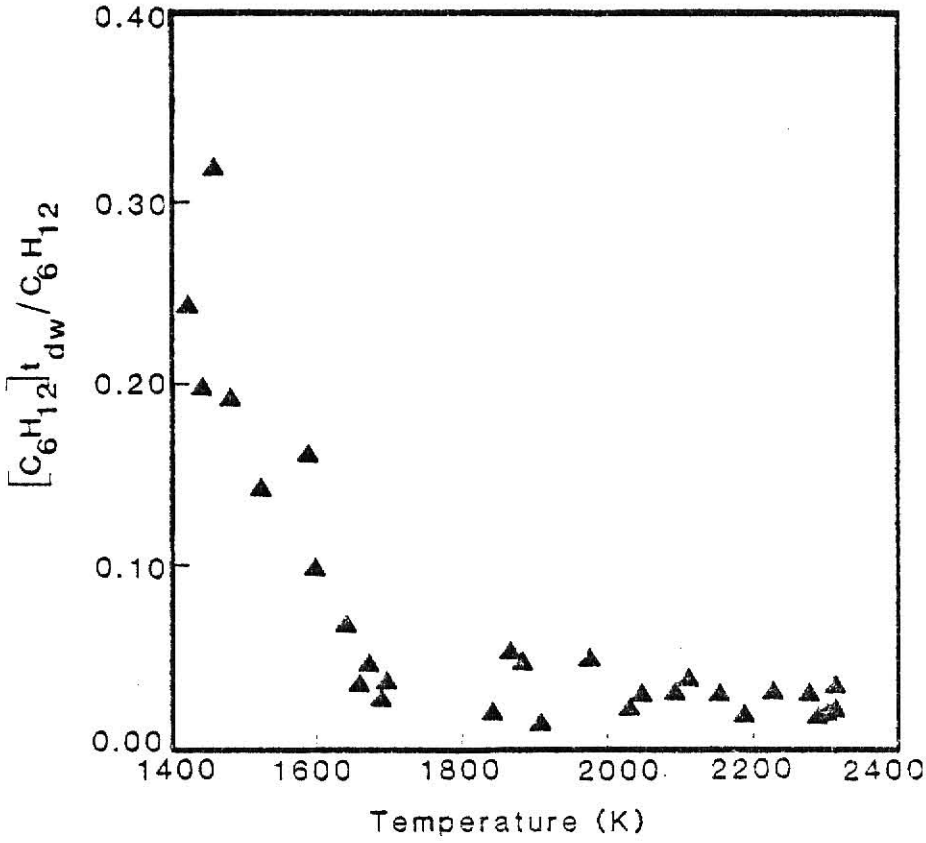

Fig. 3.1 Percent of cyclohexane remaining after pyrolysis of 1.3 mol% cyclohexane in argon as a function of reaction temperature for runs with dwell times of 1.0-1.5 msec (non soot runs)

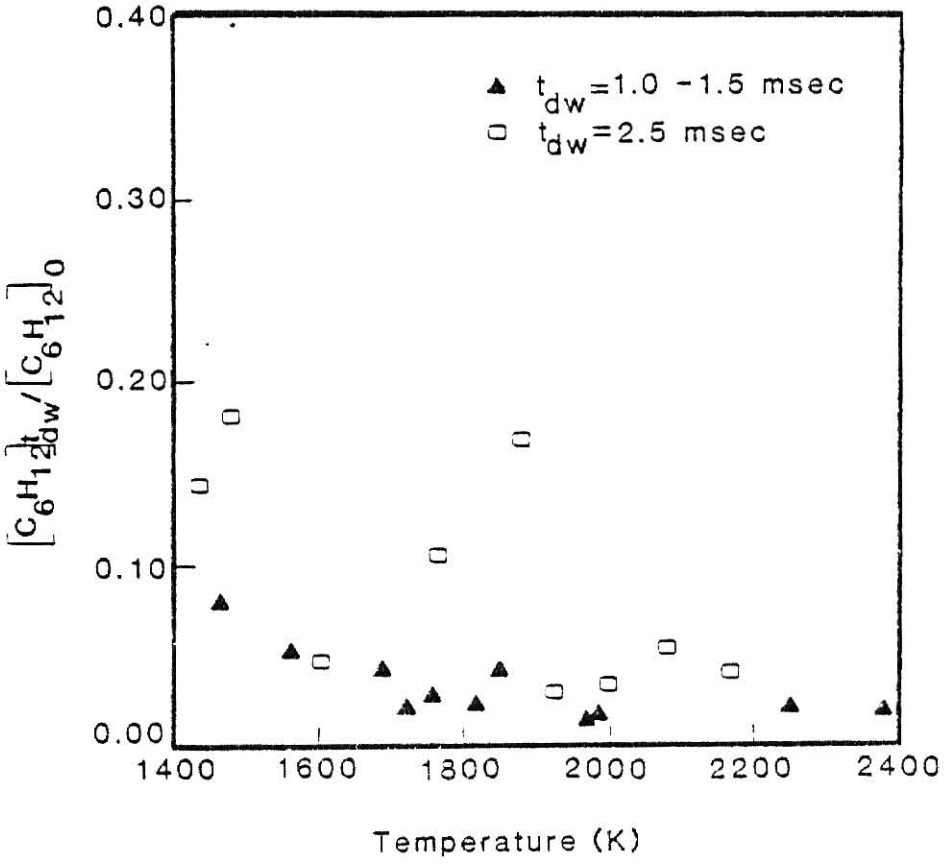

Fig. 3.2 Percent of cyclohexane remaining after pyrolysis of 1.3 mol% cyclohexane in argon as a function of reaction temperature for experiments designated as soot runs

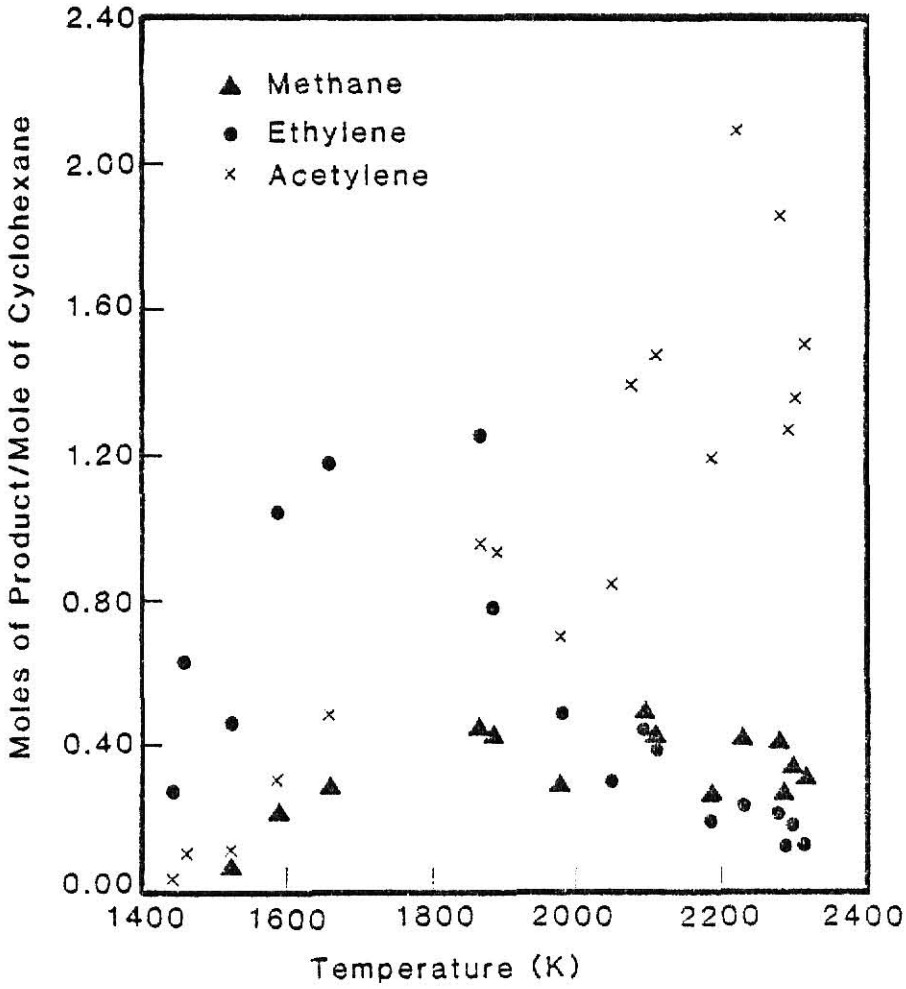

Fig. 3.3 Product yields from the pyrolysis of 1.3 mol% cyclohexane in argon as a function of reaction temperature for non soot runs with dwell times of 1.0-1.5 msec

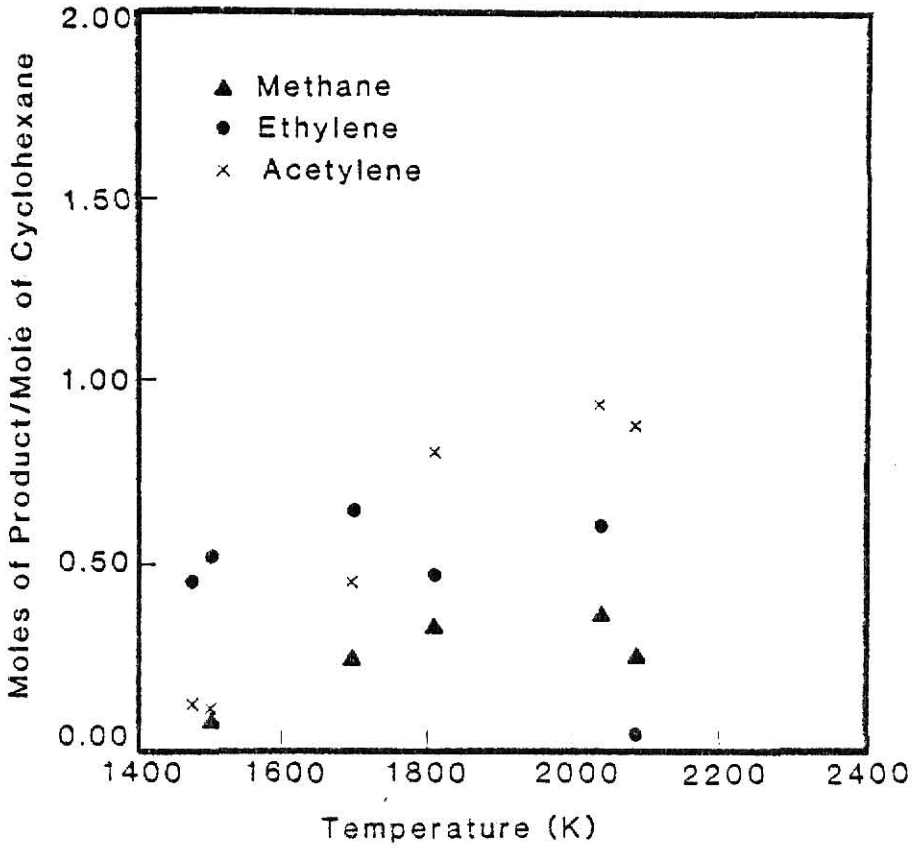

Fig. 3.4 Product yields as a function of temperature for the pyrolysis of 0.8 mol% cyclohexane in argon

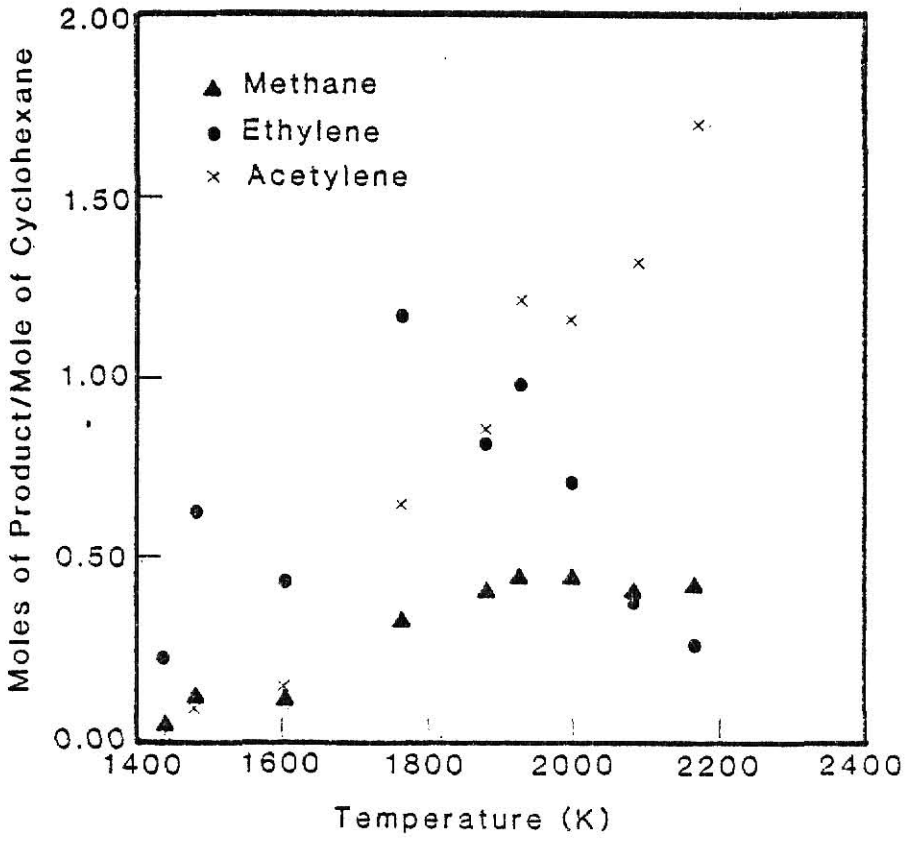

Fig. 3.5 Product yields from the pyrolysis of 1.3 mol% cyclohexane in argon with dwell times of 1.0-1.5 msec and designated as soot runs

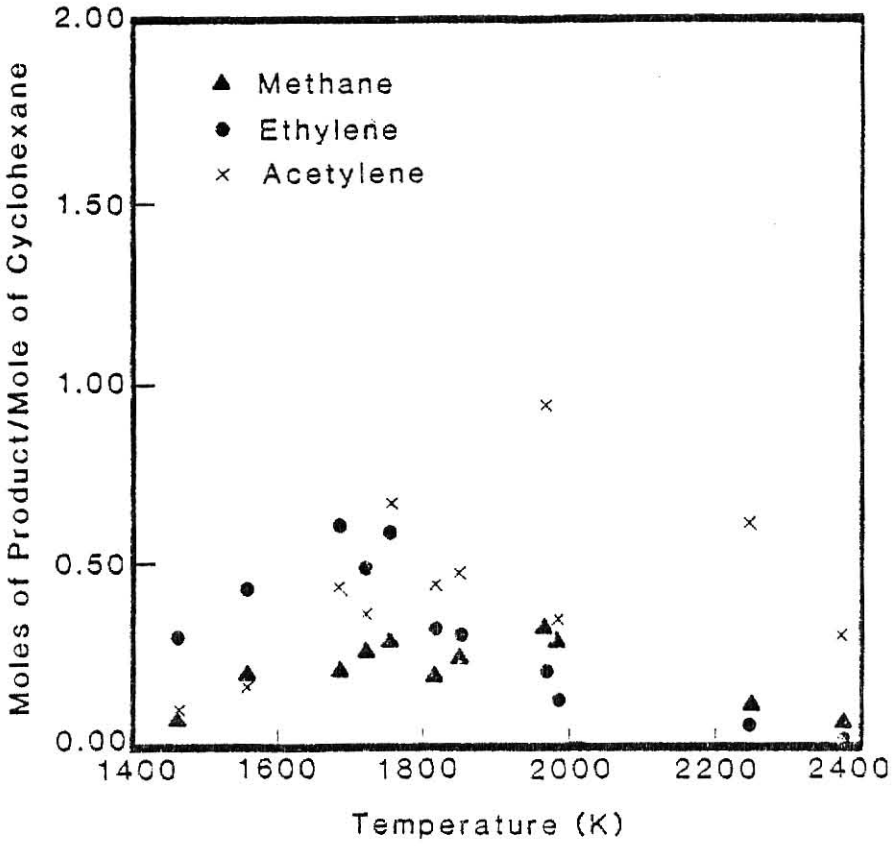

Fig. 3.6 Product yields as a function of temperature for the pyrolysis of 1.3 mol% cyclohexane in argon with dwell times near 2.5 msec and designated as soot runs

non-soot runs, the yields of methane and ethylene peak near 1900 K. Other products whose yields were examined were hydrocarbons with three and four carbon atoms. The C_3 compounds were ascertained to be propene and propyne, while one of the C_4 products was found to be 1,3-butadiene. The remaining C_4 species was reasoned to be 1,2-butadiene, for it appeared between 1-butyne and 2-butyne and before 1,3-butadiene on the gas chromatogram. Comparison of the heats of formation of these compounds reveals that 1,2-butadiene is more stable than 1-butyne by about 1 kcal/mole, but less stable than 2-butyne by 4 kcal/mole, and almost 13 kcal/mole less stable than 1,3-butadiene.[16] The C_3 and C_4 product yields are plotted in Fig. 3.7. The compound with the greatest yield for this set of products is 1,3-butadiene. Propene and propyne reach maximum yields at about 1600 K, and the 1,2-butadiene peaks at about 1800 K. Traces of benzene were also found in the pyrolyzed gases, but only in quantities near the detectable limit (1×10^{-9} g). Certain data obtained from the 0.8 mol% and 0.4 mol% mixtures appear questionable. There exists the possibility that the detector efficiency for low concentrations of certain hydrocarbons is too low to yield reliable results, and so these data have been neglected in any further analysis.

3.1.2 Benzene

Pyrolysis of 1.3 mol% benzene in argon resulted in gaseous products consisting of methane and acetylene, with traces of ethylene. Results for the benzene pyrolysis experiments are listed in Table 3.3. Interpretation of the gas chromatograms revealed that there were also gaseous hydrocarbons with three to five carbon atoms; however, these

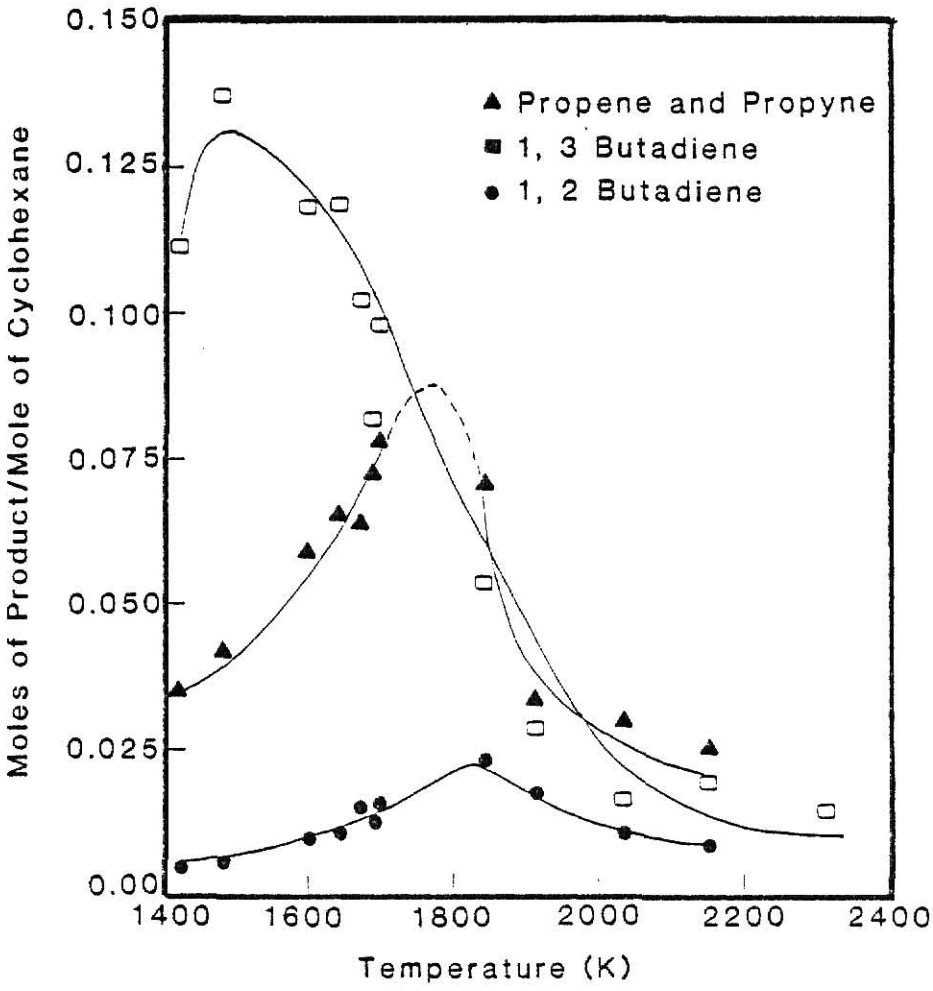

Fig. 3.7 Yields of C_3 and C_4 products as a function of reaction temperature for the pyrolysis of 1.3 mol% cyclohexane in argon with dwell times of 1.0-1.5 msec

Table 3.3. Results of analysis of gaseous products from the pyrolysis of benzene

T_5 (K)	P_5 ($\times 10^5$Pa)	t_{dw} (msec)	$[C_6H_6]_0$	$\frac{[C_6H_6]t_{dw}}{[C_6H_6]_0}$	Product yields (moles of product/mole of C_6H_6) CH_4	C_2H_4	C_2H_2
1513	12.8	1.4	0.0132	0.437	0.0165	---	0.0129
1673	12.3	1.5	0.0132	0.181	0.0260	0.00406	0.107
1829	11.5	1.5	0.0132	0.0606	0.0895	0.00583	0.300
1949	13.2	2.1	0.0132	0.0375	0.123	0.0213	0.547
2022	10.4	1.0	0.0132	0.0681	0.0636	0.00648	0.411
2249	10.1	1.0	0.0132	0.0129	0.0378	---	0.528
1397*	13.3	2.7	0.0132	0.174	0.129	0.00731	0.0472
1471*	13.0	2.8	0.0132	0.136	0.0213	0.00207	0.0351
1667*	12.2	2.7	0.0132	0.0910	0.0558	0.00868	0.194
1682*	8.9	2.1	0.0132	0.0455	0.0644	---	0.144
1830*	11.1	2.5	0.0132	0.109	0.0559	---	0.254
2048*	10.6	2.3	0.0132	0.0186	0.0424	---	0.225
2226*	10.0	2.2	0.0132	0.0661	0.0266	---	0.322
2230*	10.0	2.2	0.0132	0.00275	0.0375	---	0.391

*Soot run.

were not investigated further. Traces of toluene were also found in the samples. Figure 3.8 is a plot of the percentage of benzene remaining in the gas sample taken after pyrolysis. Figures 3.9 and 3.10 are of the yields of methane, acetylene, and ethylene versus reaction temperature for the benzene pyrolysis.

3.1.3 Benzene/Cyclohexane Mixtures

Two benzene/cyclohexane mixtures were studied using the SPST. The first was 1.36 mol% benzene/0.07 mol% cyclohexane in argon, and the other, 1.07 mol% benzene/0.36 mol% cyclohexane in argon. Data from the thermal decomposition of these mixtures are listed in Tables 3.4 and 3.5. Figures 3.11 through 3.14 show the relative amounts of the reactants remaining in the samples after pyrolysis. The yields of methane, ethylene, and acetylene are plotted against reaction temperature in Figs. 3.15-3.18. Again, C_3-C_5 compounds were present in the sample along with traces of toluene.

3.2 Solid and Liquid Residue Gravimetric Analysis

The data recorded for the gravimetric analysis of the residue appearing on the aluminum liners for shocks with a dwell time of approximately 2.5 msec appear in Tables 3.6-3.9. Figures 3.19 to 3.21 are plots of the weight percent of reactant appearing as residue on the liners as a function of reaction temperature. Problems were encountered when the ambient humidity would change greatly between the initial weighing of the liners and the after-shock weighing. Therefore, certain data had to be corrected using an average liner weight as the initial weight. These data are so indicated in the tables. The large error

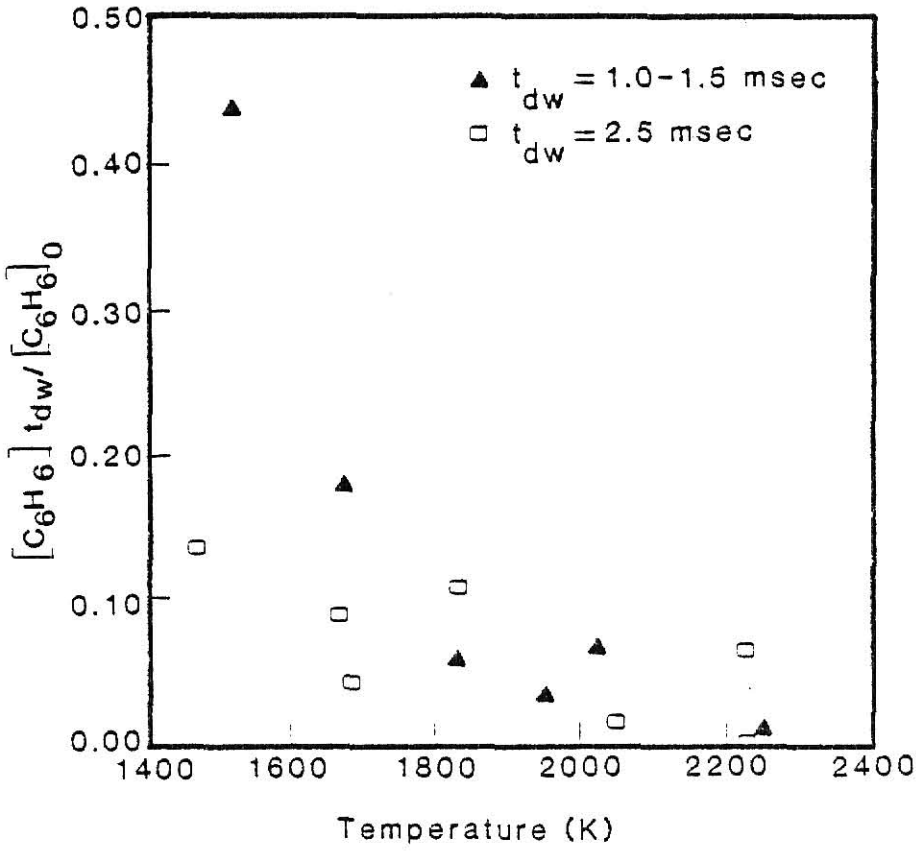

Fig. 3.8 Percent of benzene remaining after the pyrolysis of 1.3 mol% benzene in argon

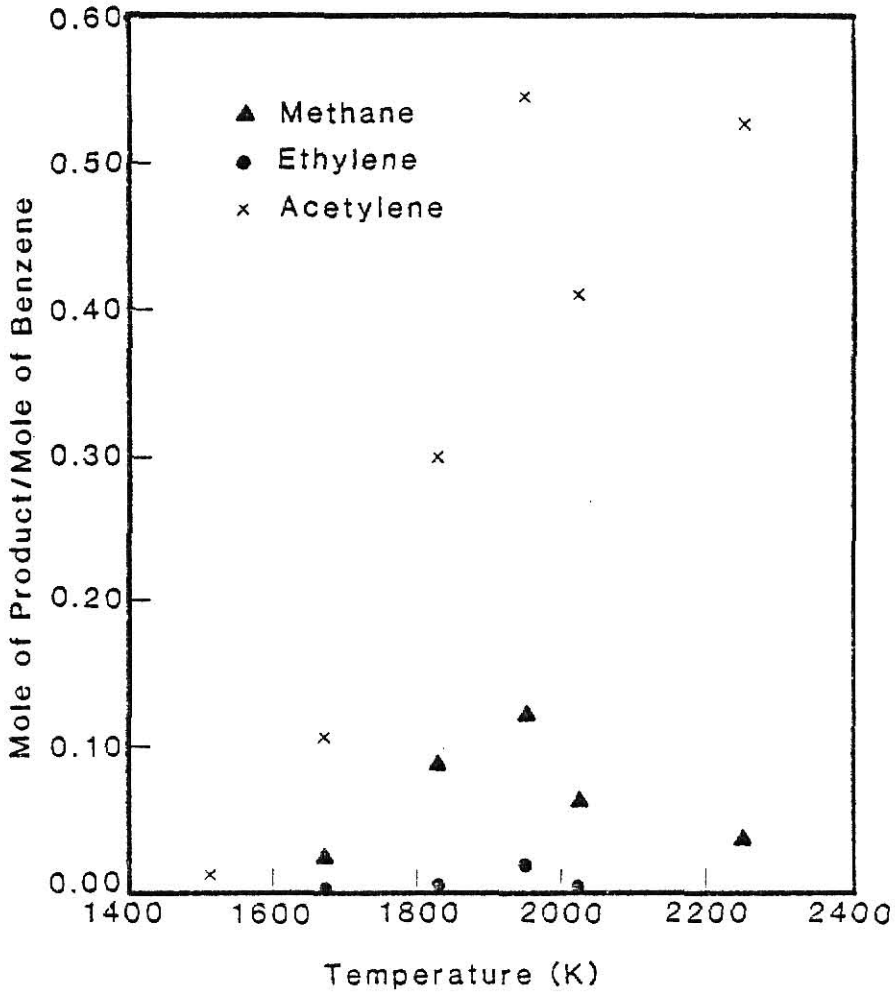

Fig. 3.9 Product yields as a function of temperature for the pyrolysis of benzene with dwell times of 1.0-1.5 msec

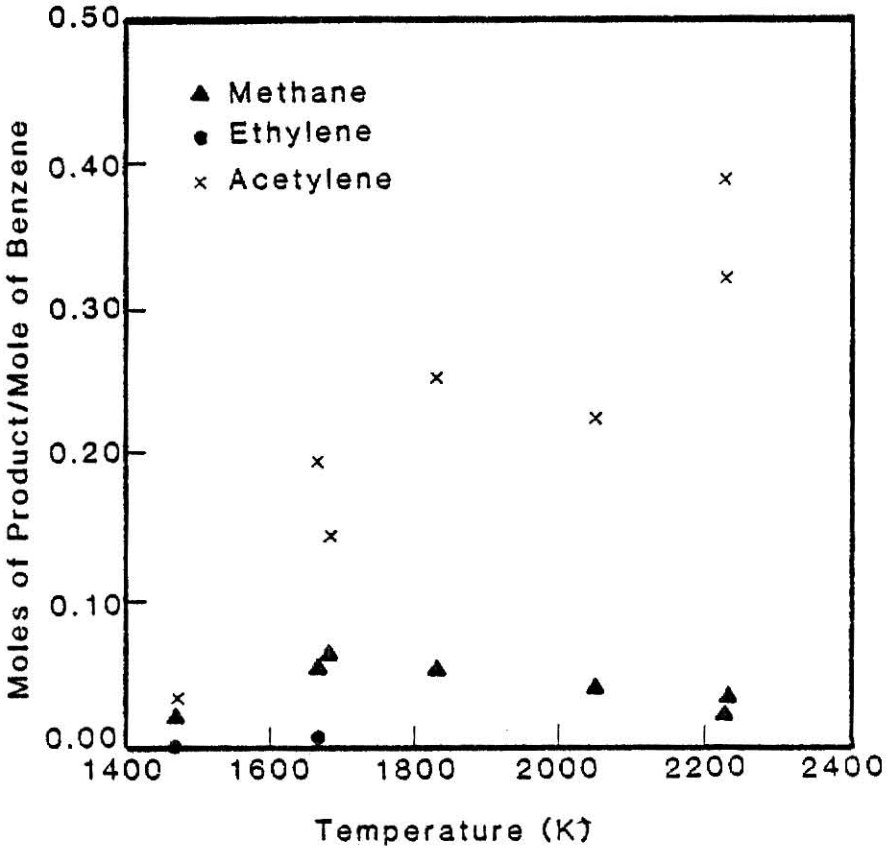

Fig. 3.10 Product yields as a function of temperature for the pyrolysis of benzene with dwell times near 2.5 msec.

Table 3.4. Gaseous product yields from the pyrolysis of 1.36 mol% benzene/0.07 mol% cyclohexane

T_5 (K)	P_5 ($\times 10^5$ Pa)	T_{dw} (msec)	$\frac{[C_6H_{12}]t_{dw}}{[C_6H_{12}]_0}$†	$\frac{[C_6H_6]t_{dw}}{[C_6H_{12}]_0}$††	(moles of product/mole of reactants) CH_4	C_2H_2	C_2H_2
1485	12.4	1.4	0.420	0.401	0.0180	0.0305	0.122
1619	12.5	1.5	0.0879	0.453	0.0428	0.0604	0.0490
1673	11.0	1.1	0.0752	0.324	0.0632	0.0620	0.0180
1928	11.4	1.1	0.0321	0.0937	0.0886	0.0225	0.276
1980	10.4	0.9	0.0331	0.116	0.126	0.0155	0.070
2140	8.8	0.7	0.0295	0.0734	0.0727	0.00894	0.588
2413	10.4	1.6	0.0319	0.0163	0.0424	0.00533	0.927
1476*	12.3	2.6	0.143	0.360	0.0382	0.0151	0.0293
1579*	12.1	2.8	0.0623	0.231	0.0548	0.0474	0.0774
1757*	12.3	2.7	0.0374	0.0345	0.0751	0.0193	0.212
1802*	11.8	2.5	0.0278	0.00449	0.0654	0.00455	0.210
1847*	11.2	2.5	0.0313	0.0417	0.0471	0.00373	0.172
2043*	11.8	2.5	0.0383	0.0193	0.0662	0.00710	0.500
2100*	11.0	2.4	0.0361	0.0578	0.0581	---	0.490
2268*	10.2	2.1	0.0762	0.0196	0.0347	---	0.283

*Soot run.

†$[C_6H_{12}]_0 = 0.0007$.

††$[C_6H_6]_0 = 0.0136$.

Table 3.5. Gaseous product yields from the pyrolysis of 1.07 mol% benzene/0.36 mol% cyclohexane

T_5 (K)	P_5 ($\times 10^5$ Pa)	T_{dw} (msec)	$\frac{[C_6H_{12}]t_{dw}}{[C_6H_{12}]_0}$†	$\frac{[C_6H_6]t_{dw}}{[C_6H_{12}]_0}$††	(moles of product/mole of reactants) CH_4	C_2H_2	C_2H_2
1730	11.1	1.7	0.0265	0.0629	0.232	0.178	0.436
1874	10.9	1.1	0.0257	0.0808	0.325	0.194	0.745
2027	10.5	1.1	0.0551	0.0121	0.205	0.0452	0.699
2177	10.3	1.3	0.0521	0.0189	0.163	0.0281	0.052
2322	9.9	1.3	0.0247	0.0226	0.0698	---	0.716
1383*	13.1	2.7	0.1411	0.0884	0.0435	0.168	0.0407
1483*	12.4	2.7	0.0749	0.243	0.0631	0.261	0.144
1510*	13.9	2.9	0.0679	0.109	0.115	0.216	0.151
1601*	12.3	2.9	0.0414	0.0637	0.168	0.224	0.275
1660*	11.3	2.7	0.0355	0.0507	0.179	0.154	0.329
1807*	11.8	2.5	0.0480	0.0484	0.186	0.0625	0.497
1844*	10.1	2.5	0.0278	0.0382	0.165	0.0483	0.391
1885*	10.0	2.3	0.0361	0.0447	0.162	0.0428	0.448
2074*	10.8	2.3	0.156	0.0157	0.112	0.0237	0.471
2116*	9.9	2.2	0.148	0.00983	0.0838	---	0.336

*Soot run.

†$[C_6H_{12}]_0 = 0.0036$.

††$[C_6H_6]_0 = 0.0107$.

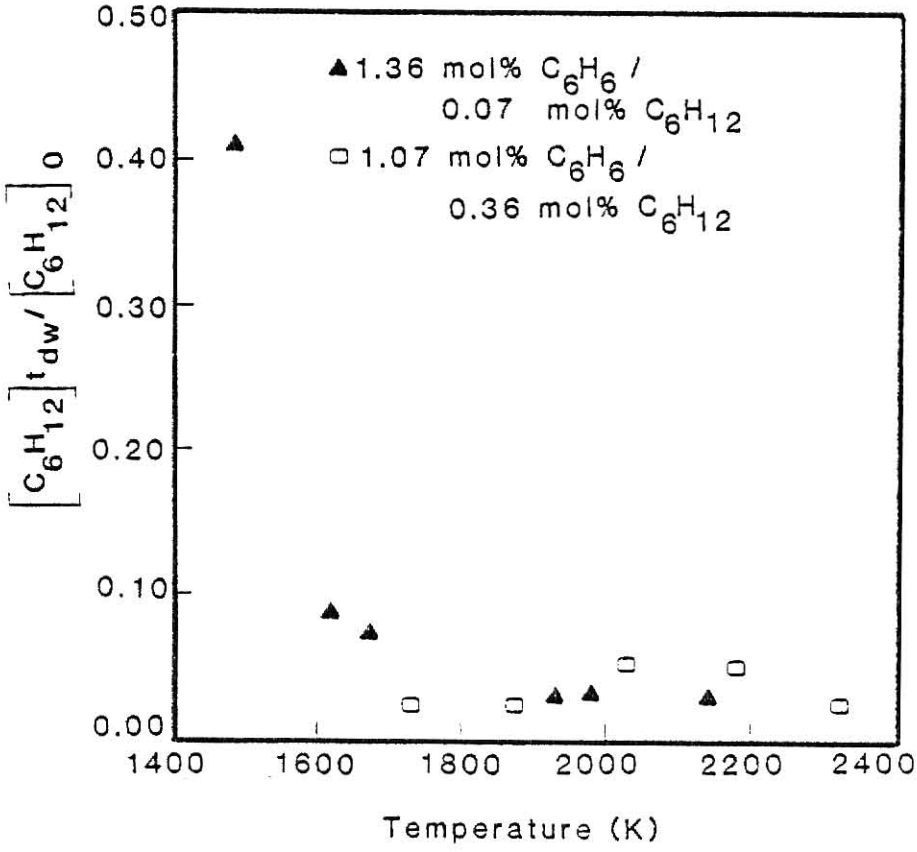

Fig. 3.11 Percent of cyclohexane remaining after pyrolysis of benzene/cyclohexane mixtures with dwell times of 1.0-1.5 msec.

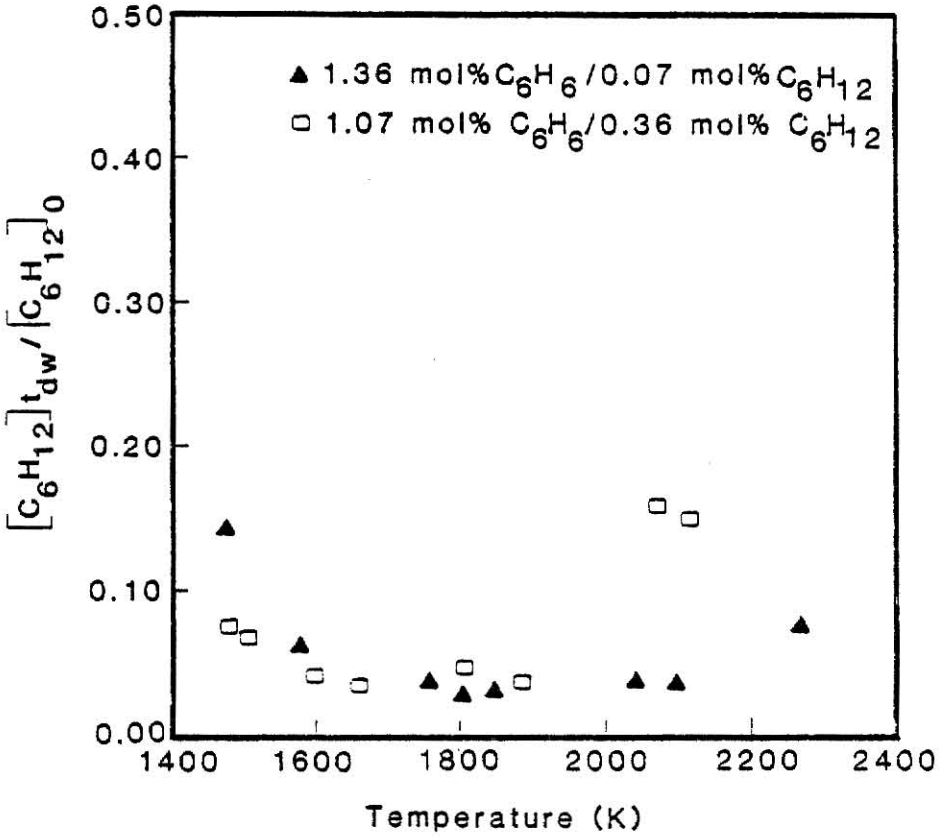

Fig. 3.12 Percent of cyclohexane remaining after pyrolysis of benzene/cyclohexane mixtures with dwell times near 2.5 msec.

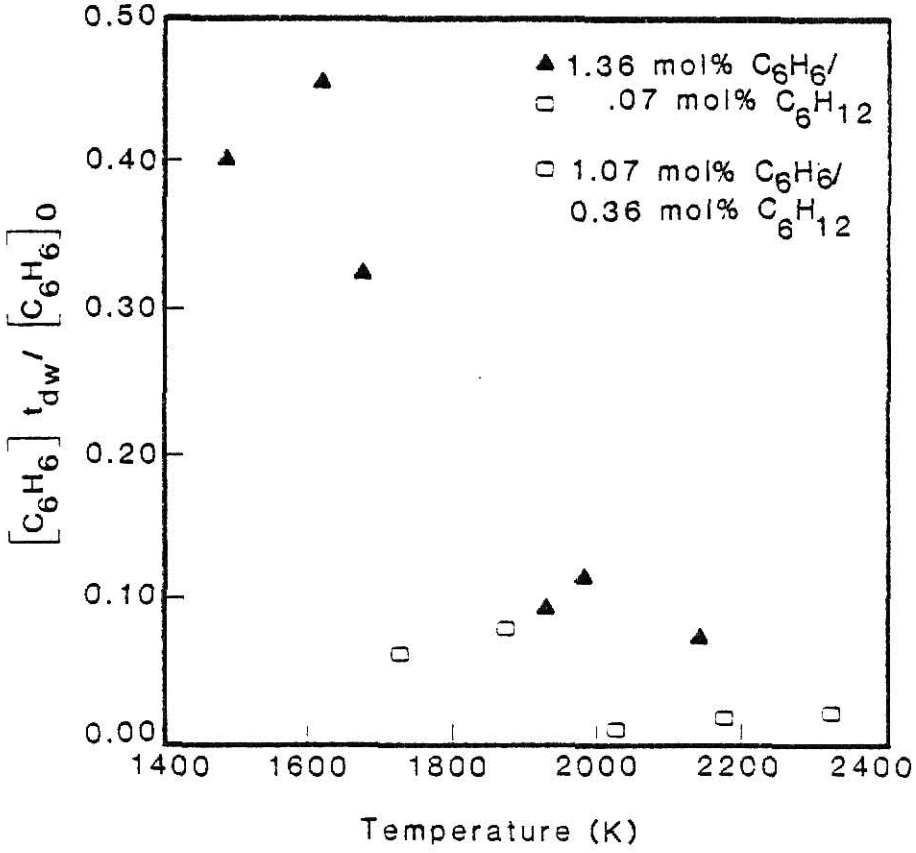

Fig. 3.13 Percent of benzene remaining as a function of reaction temperature for benzene/cyclohexane mixtures with dwell times of 1.0-1.5 msec.

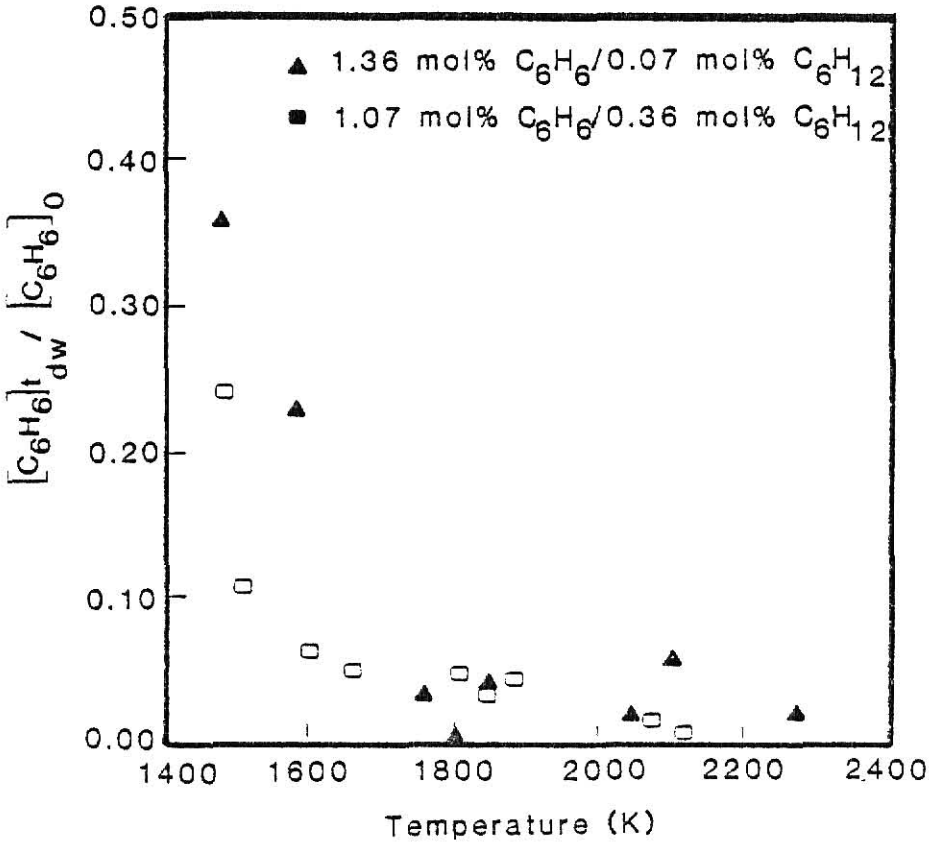

Fig. 3.14 Percent of benzene remaining as a function of reaction temperature for benzene/cyclohexane mixtures with dwell times near 2.5 msec.

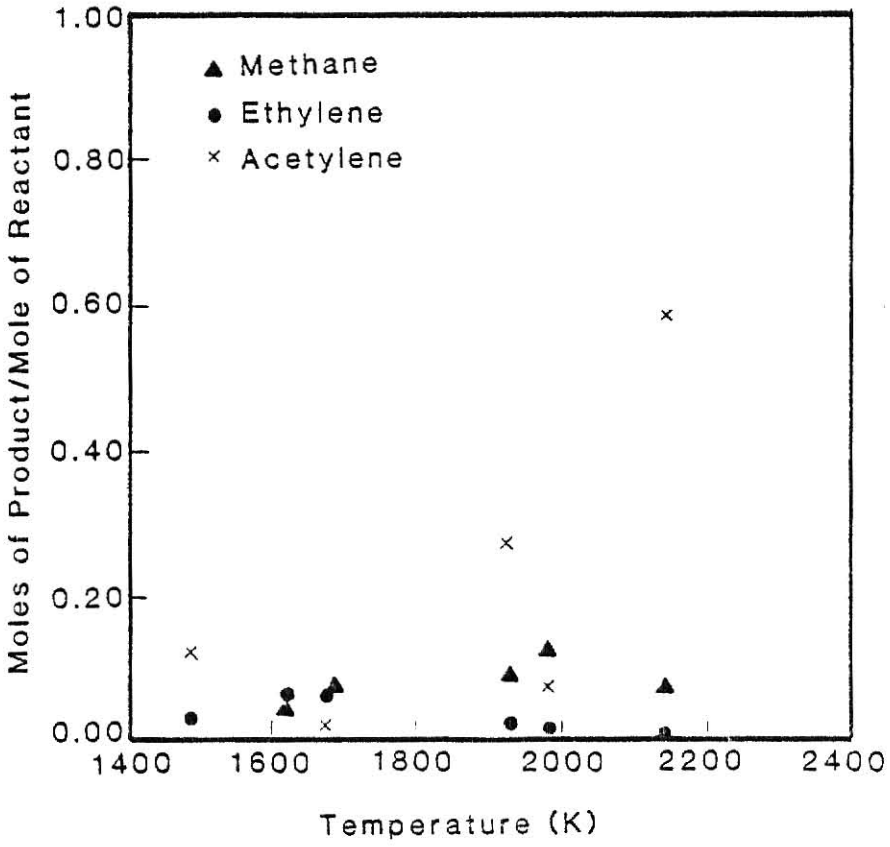

Fig. 3.15 Product yields as a function of temperature for the pyrolysis of 1.36 mol% benzene/ 0.07 mol% cyclohexane in argon with dwell times of 1.0-1.5 msec.

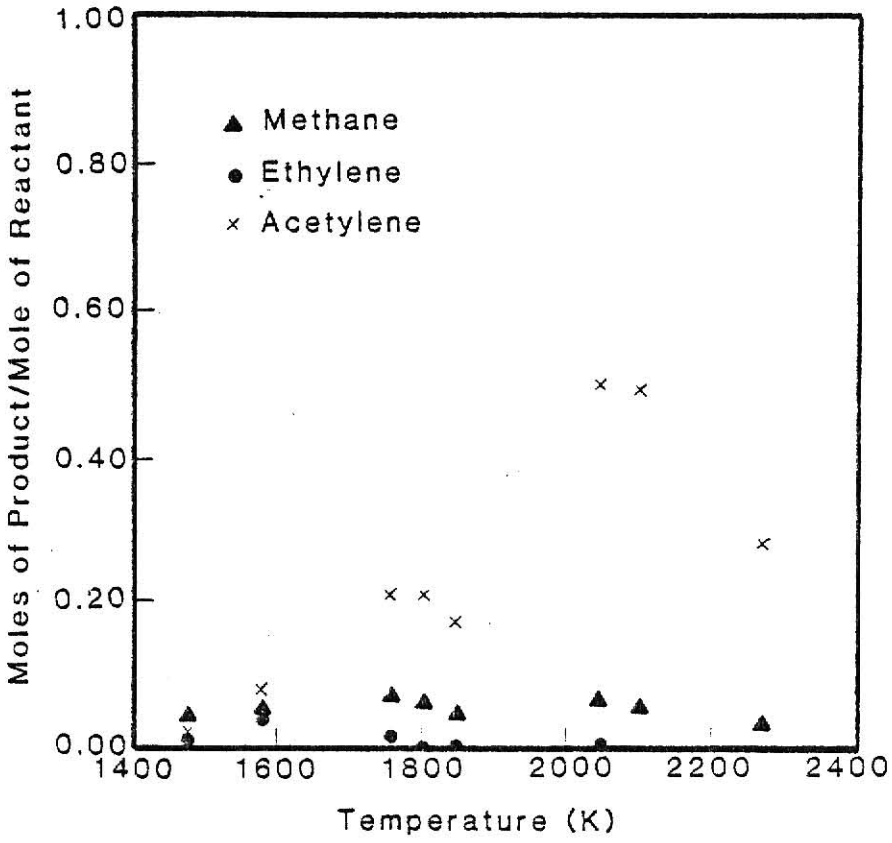

Fig. 3.16 Product yields as a function of temperature for the pyrolysis of 1.36 mol% benzene/ 0.07 mol% cyclohexane in argon with dwell times near 2.5 msec.

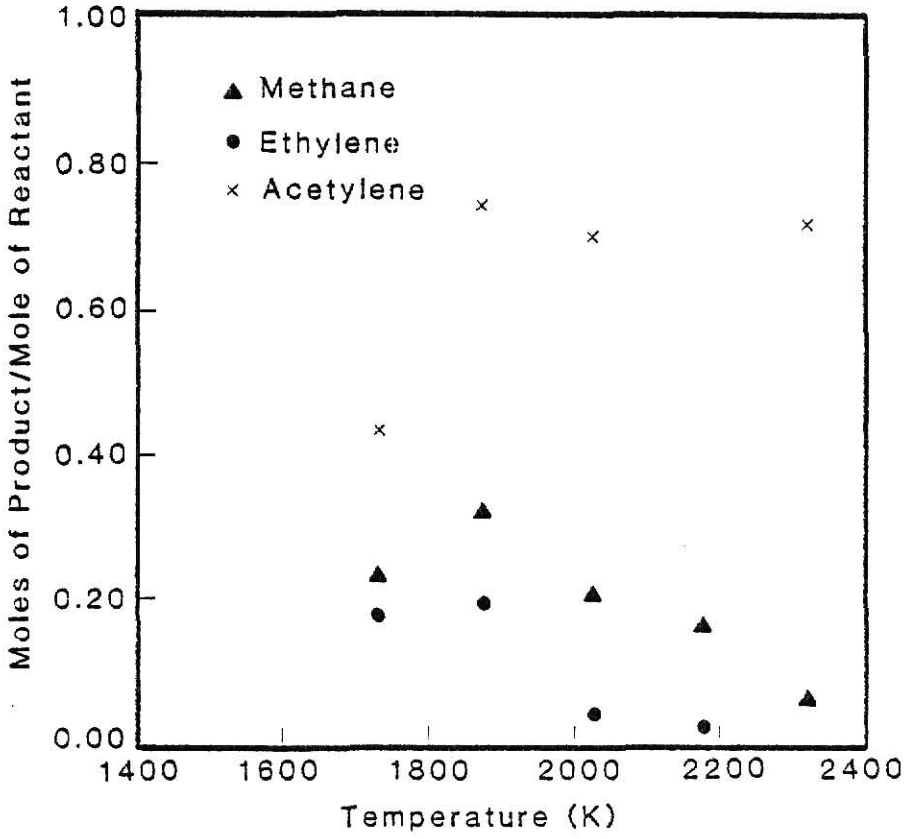

Fig. 3.17 Product yields as a function of temperature for the pyrolysis of 1.07 mol% benzene/ 0.36 mol% cyclohexane in argon with dwell times of 1.0-1.5 msec.

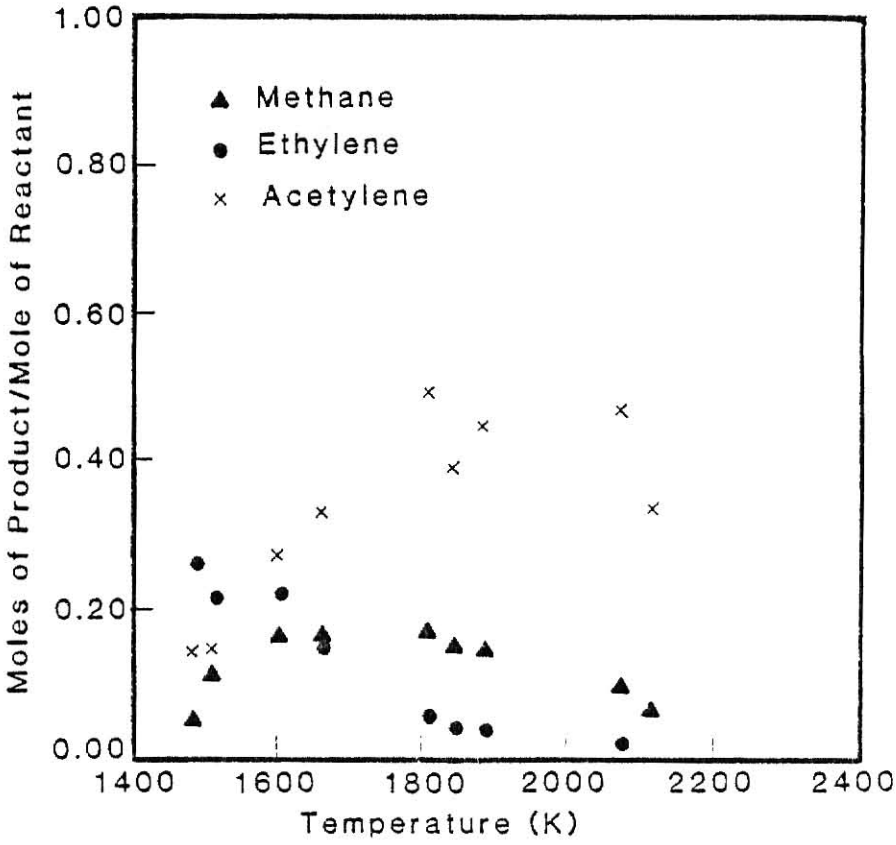

Fig. 3.18 Product yields as a function of temperature for the pyrolysis of 1.07 mol% benzene/ 0.36 mol% cyclohexane in argon with dwell times near 2.5 msec.

Table 3.6. Residue yields from cyclohexane pyrolysis

T_5 (K)	T_{dw} (msec)	Mass fractional yield	Comments
1463	2.0	0.131	no visible residue
1558	2.4	0.148	
1685	2.2	0.109	
1694	2.6	0.157	
1721	2.7	0.107	no visible residue
1756	2.7	0.410	
1817	2.3	0.373	
1852	2.5	0.360	slight white cast
1970	2.7	0.337	white-gray residue
1982	2.5	0.367	solid is light brown in color
1985	2.4	0.534	gray-brown residue
2121	2.3	0.635	brown-black solid
2140	2.3	0.320	
2249	2.3	0.532	black solid
2376	2.3	0.841	black particulate solid

Table 3.7. Residue yields from benzene pyrolysis

T_5 (K)	T_{dw} (msec)	Mass fractional yield	Comments
1397	2.7	0.110	no visible residue
1471	2.8	0.137	
1667	2.7	0.278	white-gray residue
1682	2.1	0.182	white-gray residue
1830	2.5	0.484	gray-brown solid residue
2048	2.3	0.476	brown-black residue
2226	2.2	0.571*	black residue

*Yield corrected for moisture.

Table 3.8. Residue yields from pyrolysis of 1.36 mol% benzene/0.07 mol% cyclohexane

T_5 (K)	T_{dw} (msec)	Mass fractional yield	Comments
1476	2.6	.483	no visible residue
1579	2.8	.135	
1680	2.5	.367	white-gray residue
1757	2.7	.321	white-gray residue
1802	2.5	.556	brown solid residue
1847	2.5	.375	
2047	2.5	.405*	
2100	2.4	.384	brown-black solid residue
2268	2.1	.334	

*Yield corrected for moisture.

Table 3.9. Residue yields from pyrolysis of 1.07 mol% benzene/0.36 mol% cyclohexane

T_5 (K)	T_{dw} (msec)	Mass fractional yield	Comments
1383	2.7	0.0824	no visible residue
1483	2.7	0.104*	
1510	2.9	0.242	
1601	2.9	0.487	
1660	2.7	0.362	no visible residue
1807	2.5	0.412	white-gray residue
1844	2.5	0.518	gray-brown residue
1885	2.3	0.496	brown residue
2074	2.3	0.562	black residue-fine particles
2116	2.2	0.500	black residue

*Yield corrected for moisture.

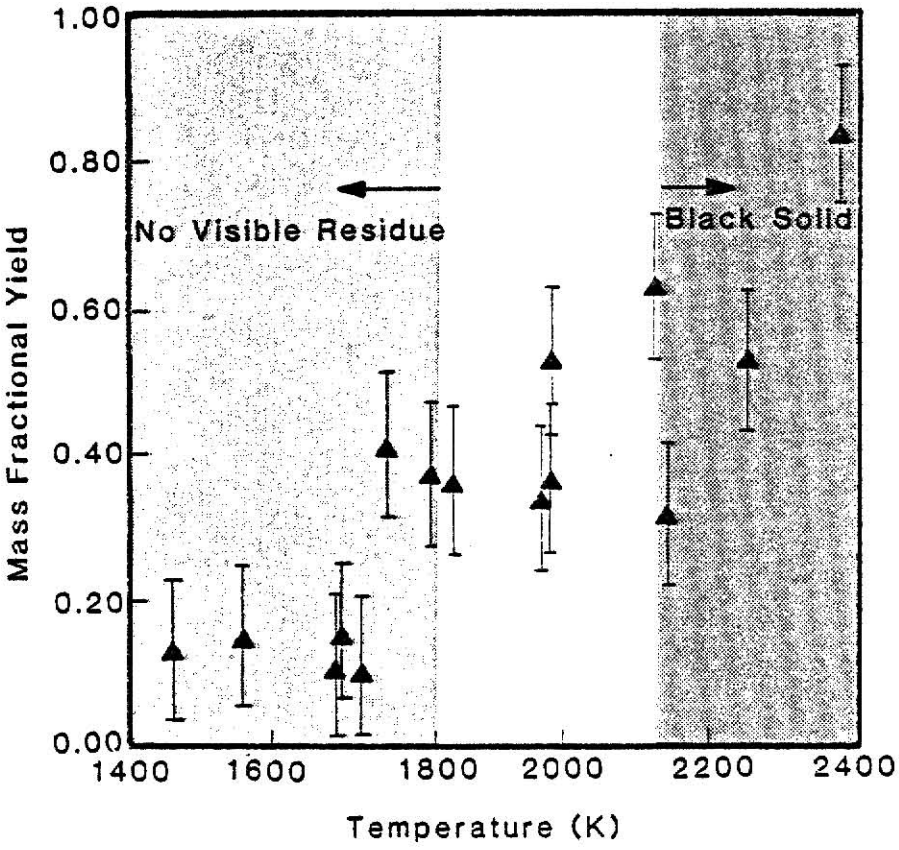

Fig. 3.19 Mass fractional yields of residue as a function of temperature for the pyrolysis of 1.3 mol% cyclohexane in argon with dwell times near 2.5 msec.

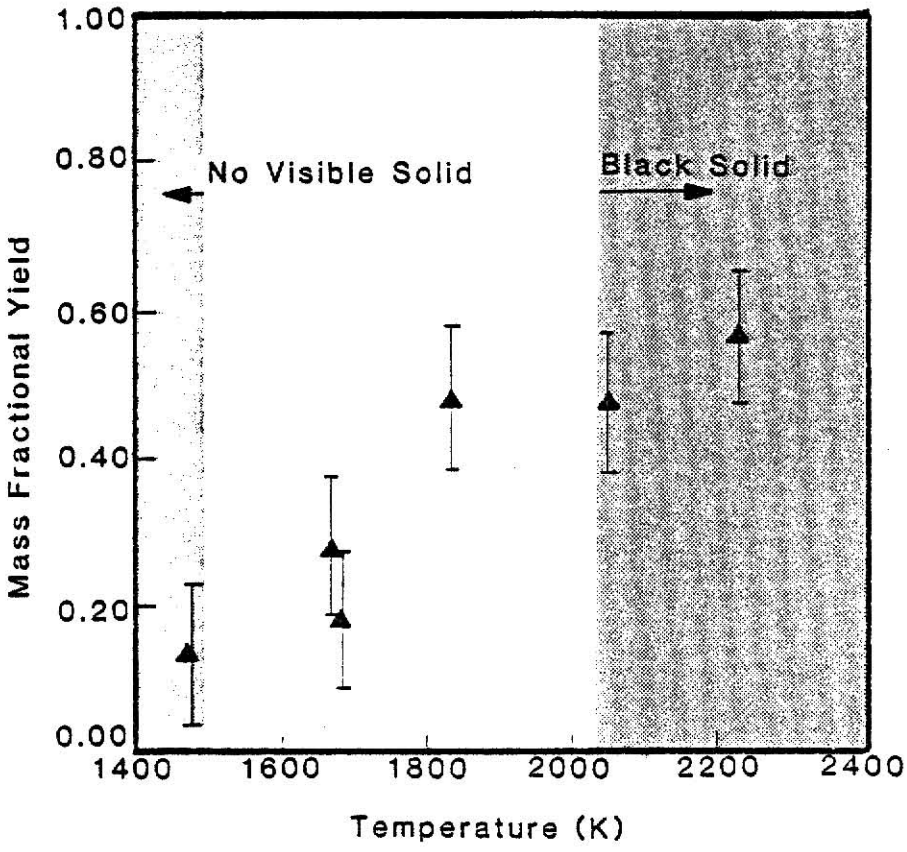

Fig. 3.20 Mass fractional yield of residue as a function of temperature for the pyrolysis of 1.3 mol% benzene in argon

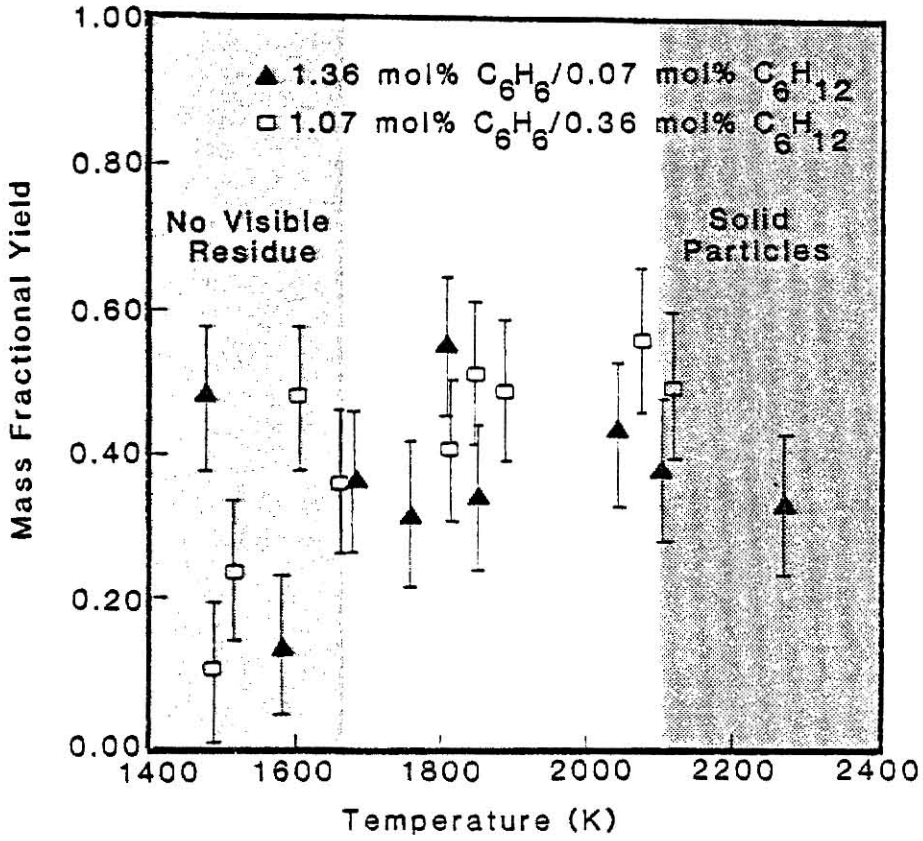

Fig. 3.21 Mass fractional yield of residue as a function of temperature for the pyrolysis of benzene/cyclohexane/argon mixtures

bars are necessitated by the difficulty of measuring milligram quantities of residue on the much heavier liners. The method with which they were obtained is discussed in Appendix C.

4.0 DISCUSSION

4.1 Global Kinetics of Cyclohexane

A global rate constant for the thermal decomposition of cyclohexane was determined from the data collected for experiments with a dwell time of 1.5 msec or less and a reaction temperature of less than 1700 K. The decomposition was assumed to be first order in remaining cyclohexane,[21,24] since the amount of data used in the calculation of the global rate constant was considered insufficient to allow determination of the reaction order.

If the temperature dependence of the frequency factor, A, is neglected, the rate constant can be described by the Arrhenius equation,

$$k = A(\exp(-E_a/RT)), \tag{4.1}$$

where E_a is the activation energy of the reaction, R is the universal gas constant, and T, the reaction temperature. For a first order reaction, the integrated rate equation is[34]

$$K_1 = \frac{-1}{t} \ln \frac{C_t}{C_0}, \tag{4.2}$$

where t is the time during which the reaction is taking place, C_t is the concentration of the reactant at time t, and C_0 is the initial reactant concentration. The reaction time t must take into account reactions occurring during the cooling of the system. A correction for the finite cooling rate concerns adding a term to the dwell time, t_{dw}. This finite cooling rate correction is discussed in Appendix A.

A least squares fit to the data, along with the finite cooling rate correction, yielded a global rate constant for the decomposition of

cyclohexane of

$$k_1 = (1.2 \times 10^5) \exp(-7215/T) \text{ sec}^{-1}. \qquad (4.3)$$

Thus, the activation energy is calculated to be 14.3 kcal/mole. The rate of decomposition of cyclohexane did not appear to be affected by the presence of benzene.

4.2 Gaseous Products

Comparison of the results of the current study to the products of the decomposition of cyclohexane as observed by Virk,[20] Tsang,[21] and Shevel'kova et.al.,[19] discloses agreement that the products include methane, ethylene, acetylene, 1,3-butadiene, propene, and propyne. However, the constituent determined to be 1,2-butadiene was not reported as being present in the product gases by the other researchers. Also, 1-hexene, given by Tsang as the product of the initiation step in the decomposition of cyclohexane, was not detected. If 1-hexene is a result of the initial step, one possible reason for the lack of this constituent in the products is the high reaction temperatures employed in this study, which cause the 1-hexene to decompose rapidly.

When a radical is allowed to react with a cyclohexane molecule, a cyclohexyl radical can result. Tsang[23] stated that a possible decomposition pathway for the cyclohexyl radical is

(a) Cyclopentylmethyl

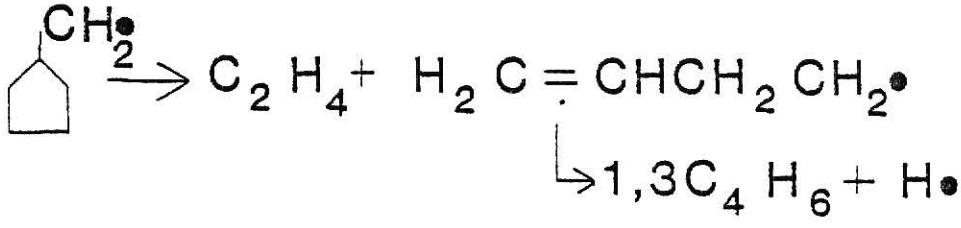

(b) 3-methyl-cyclopentyl-1

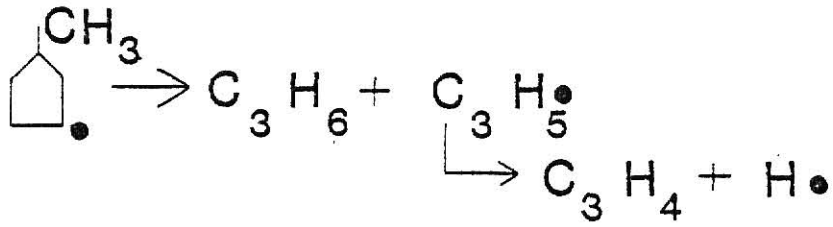

(c) 1-methyl-cyclopentyl-1

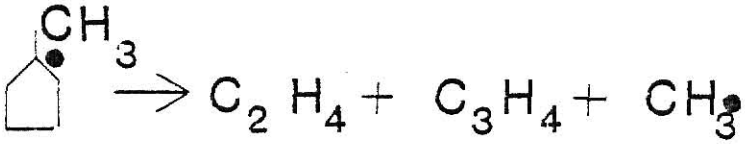

(d) 2-methyl-cyclopentyl-1

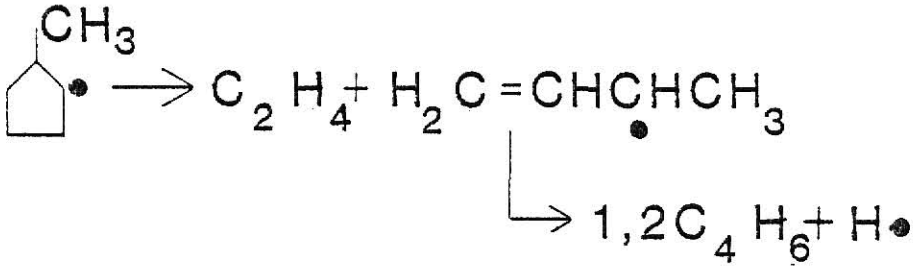

Fig. 4.1 Mechanisms for the decomposition of methylcyclopentyl radicals

The presence of methylcyclopentyl radicals in the decomposition mechanism may account for the occurrence of 1,2-butadiene in the pyrolysis products. Tsang shows only two forms of the methylcyclopentyl radical, cyclopentylmethyl and 3-methyl-cyclopentyl-1; however, other forms of the radical do exist. Two other conformations of $C_6H_{11}\cdot$ are 1-methyl-cyclopentyl-1 and 2-methyl-cyclopentyl-1. Figure 4.1 shows possible mechanisms, based on the product distributions disclosed in Chapter 3, for the breakdown of these methylcyclopentyl radicals. Reactions (a) and (b) can be compared to those proposed by Tsang, shown in Fig. 1.2. Santanova, et al.,[24] presented C_4H_7 as one of the products from the decomposition of radicals with five-membered rings. If the stabilities of the radicals, based on configuration, are ranked as cyclopentylmethyl as the least stable, then 3-methyl-cyclopentyl-1, 2-methyl-cyclopentyl-1, and 1-methyl-cyclopentyl-1 as the most stable, the proposed mechanisms account for the trends in the yields of C_3 and C_4 products, as seen in Fig. 3.7. The yield of 1,3-butadiene peaks at about 1500 K, and then decreases with increasing temperature. Furthermore, maxima are observed for propene and propyne at about 1700 K, and near 1900 K for 1,2-butadiene. The order of the appearance of the peaks, assuming 1,3-butadiene reaches a maximum at a low temperature, is compatible with the breakdown of the methylcyclopentyl radicals. The least stable radical yields $1,3C_4H_6$, the next, the C_3 compounds, and the second most stable, the $1,2C_4H_6$. Allene (C_3H_4) was not observed, possibly because of the stability of the radical or because the amount of radical formed was not sufficient to yield a detectable concentration of allene.

The pyrolysis of benzene and benzene/cyclohexane mixtures yielded methane, ethylene, and acetylene (see Tables 3.3-3.5). The benzene did not appear to affect the decomposition of cyclohexane. What is more surprising is that the more easily disrupted cyclohexane did not appreciably alter the decomposition of benzene (see Figs. 2.11-3.14). Neither did the product yields of each appear to be greatly affected by the presence of the second reactant. At least for the conditions studied in this work, the aliphatic and aromatic molecules undergo decomposition unaffected by the presence of each other. This, however, may not be the case if the concentrations of the reactants were to be increased, for which the probability of a collision occurring between the aliphatic and aromatic molecules would be greatly enhanced.

All of the products resulting from the thermal decomposition of cyclohexane can react to form acetylene. An important result of the analysis of the C_4 gaseous products is that there were no indications of the presence of such compounds as diacetylene or vinylacetylene, nor were these species detected in the pyrolysis products of benzene. This is in disagreement with Vaughn,[27] who observed trace amounts of diacetylene, vinylacetylene, and styrene as products resulting from the pyrolysis of benzene in a single pulse shock tube. Vaughn analyzed samples on a mass spectrometer, while the gas chromotograph was used in this study. The duacetylene and the vinylacetylene could have decomposed on the column in the gas chromatograph and were not detected.

4.3 Solid and Liquid Residues

Examination of Figs. 3.19 and 3.20 reveals no difference between the residue yields from the pyrolysis of the alicyclic aromatic systems. However, as noted in Tables 3.6-3.9, there does exist a distinction

concerning the visual appearance of the residue. At low temperatures, a residue was weighed, but was not seen in either system. From this, we may conclude that the residue was composed principally of liquids. An important difference between the reactants appears to be the temperature at which a visible residue begins to form. The first visible residue was white-gray in color and possessed a sheen. For cyclohexane, such a color occurred first at about 1900 K; however, the benzene yielded this color residue at 1650 K. Furthermore, the experiments revealed that the white-gray residue formed near 1700 K for the 1.36 mol% benzene/0.07 mol% cyclohexane mixture, and at 1800 K for the 1.07 mol% benzene/0.36 mol% cyclohexane mixture. The darkening in color of the residue with the increase in reaction temperature is indicative of the increase in the amount of solids present. The color change suggests a decreasing hydrogen/carbon ratio of the residue. Such a color change was also observed by Gordon, et al.[35] during the pyrolysis of methane in hydrogen. Carbon deposits formed at low concentrations were a lustrous dense product and changed to a product which appeared dull and loose, containing particles of carbon black, at higher concentrations.

5.0 CONCLUSIONS AND RECOMMENDATIONS

Comparison of the acetylene yields for the experiments with dwell times of 1.0-1.5 msec to those with dwell times of 2.5 msec reveals that yields of the long dwell time experiments are lower at temperatures above 1800 K (see Figs. 3.3, 3.6, 3.9, and 3.10). The trend is true for both cyclohexane and benzene pyrolysis, but is more pronounced in the cyclohexane experiments. If the view is taken that the formation of an aromatic is needed to begin the sooting process, it is possible that the acetylene produced in the decomposition of cyclohexane further reacts to form benzene or higher aromatics. Traces of benzene were, in fact, detected in the samples from cyclohexane pyrolysis. In the benzene system, the aromatic is already present and need not be formed. A mechanism including methylcyclopentyl radicals in the pathway accounts for the pyrolysis products observed and their order of appearance as a function of reaction temperature during the thermal decomposition of cyclohexane. Comparison of the gaseous product yields from the pyrolysis of cyclohexane to those from the pyrolysis of benzene and benzene/cyclohexane mixtures shows that the alicyclic and aromatic systems act independently. Though acetylene is present, the lack of diacetylene and vinylacetylene in the pyrolysis products does not support a model of soot formation wherein these compounds are important precursors in soot formation. This absence of polyacetylenes along with the results of the solid and liquid residue gravimetric analysis supports a soot model in which liquid droplets of polyaromatic hydrocarbons act as precursors to soot. The absence of PAH in the gaseous analysis may be explained by the process by which the droplets

form: a supersaturated vapor condenses, leaving few PAH in the vapor phase available for detection by gas chromatographic techniques. The pathway to soot with PAH droplets as the initial step also accounts for the appearance of solids at lower temperatures for the aromatic reactant than for the aliphatic. The aromatic ring serves the purpose of a starting point for the formation of PAH. The increase in residue yields at temperatures below 1800 K from the aromatic/alicyclic systems as compared to the pure systems may indicate that stabliziation by aromatic rings of radicals formed from non-aromatic hydrocarbons as proposed by Bittner and Howard[12,36] is indeed a viable mechanism for the formation of soot. Such a mechanism leads to the formation of PAH and explains the behavior of pure as well as mixed hydrocarbon systems.

It would be beneficial to the understanding of the sooting process if qualitative analyses of the solid and liquid pyrolysis products of aliphatic and aromatic reactants could be accomplished. Another possibility for further study is to conduct experiments with various dwell times to determine if PAH are present in a vapor phase at very short dwell times. The addition of straight chain hydrocarbons to a system of alicyclic and aromatic hydrocarbons would also be of interest, since cyclic compounds lower than cyclohexane decompose into straight chain products. Tagging of organic molecules with C^{13} might lead to a determination of the initial step of soot formation. If it is determined that the presence of both radical fragments and aromatic rings are important to begin the sooting process, the optimum ratio of aliphatic to aromatic fuel components that would provide the lowest production of soot would have to be found. An aspect of the combustion

of aliphatics which must be considered is that while the soot production is lower, the production of PAH may not be, and the full impact of these hydrocarbons on the environment has yet to be established.

6.0 REFERENCES

1. E.P. Seregin, A.F. Gorenkov, V.T. Bugai, V.I. Petrov, and I.G. Klyuiko, Khimiya i Tekhnologiya Topliv i Masel, 11, 43 (1980).

2. J.P. Longwell, in Alternative Hydrocarbon Fuels: Combustion and Chemical Kinetics, edited by C.T. Bowman and J. Birkeland, Progress in Astronautics and Aeronautics, Vol. 62, 1978, p. 3,.

3. C.T. Bowman and T. Corley, in The Combustion of Pulverized Coal: Pollutant Formation and Control, edited by A.F. Sarofim, G.B. Martin, W.S. Lanier, and T.W. Lester, United States Environmental Protection Agency, Chapter 5 (in press).

4. H.Gg. Wagner, in Particulate Carbon: Formation during Combustion, edited by D.C. Siegla and G.W. Smith, General Motors Research Laboratories, 1980, p. 1.

5. J. Lahaye and G. Prado, in Particulate Carbon: Formation During Combustion, edited by D.C. Siegla and G.W. Smith, General Motors Research Laboratories, 1980, p. 33.

6. J. Lahaye and G. Prado, Chemistry and Physics of Carbon, Vol. 14, edited by P.L. Walker and P.A. Thrower, (Marcel Dekker, New York, 1978), p. 168.

7. H.B. Palmer and C.F. Cullis, Chemistry and Physics of Carbon, Vol. 1, edited by P.L. Walker (Marcel Dekker, New York, 1965), p. 265.

8. J.N. Bradley and G.B. Kistiakowsky, J. Chem. Phys., 35, 264 (1961).

9. J. Abrahamson, Nature, Lond., 266, 323 (1977).

10. S.C. Graham, J.B. Homer, and J.L.J. Rosenfeld, Proc. Roy. Soc. London A, 344, 259 (1975).

11. D.B. Scully and R.A. Davies, Carbon, 9, 185 (1965).

12. J.D. Bittner and J.B. Howard, in Alternative Hydrocarbon Fuels: Combustion and Chemical Kinetics, edited by C.T. Bowman and J. Birkeland, Progress in Astronautics and Aeronautics, Vol. 62, 1978, p. 335.

13. G. Prado and J. Lahaye, in Particulate Carbon: Formation During Combustion, edited by D.C. Siegla and G.W. Smith, General Motors Research Laboratories, 1980, p. 143.

14. G. Nelson, M.S. Thesis, Kansas State University, 1981.

15. S.C. Graham, Proc. Roy. Soc. London A, 377, 119 (1981).

16. G. Prado, Doctorate of Science thesis, Center University, Haut-Rhin and Louis Pastuer University, Strasbourg, 1972.

17. A. Streitweiser and C.H. Heathcock, Introduction to Organic Chemistry (Macmillan Publishing Co., Inc., New York, 1976).

18. L.V. Shevel'kova, R.A. Kalinenko, L.M. Vedeneyeva, R.B. Satanova, and N.S. Nanetkin, Dokl. Akad. Nauk SSSR, 251 (4), 892 (1980).

19. L.V. Shevel'kova, L.M. Vedeneyeva, and R.A. Kalinenko, Neftekhimiya, 14, (2), 242 (1974).

20. P.S. Virk, A. Korosi, and H.N. Woebcke, in Thermal Hydrocarbon Chemistry, edited by A.G. Oblad, H.G. Davis, and R.T. Eddinger, Advances in Chemistry Series, No. 183, American Chemical Society, 1978, p. 67.

21. W. Tsang, Int. J. Chem. Kinet., 10, 1119 (1978).

22. S.E. Stein and B.S. Rabinovitch, J. Phys. Chem., 79 (3), 191 (1975).

23. W. Tsang, J. Phys. Chem., 76 (2), 143 (1972).

24. R.B. Satanova, R.A. Kalinenko, and N.S. Nametkin, Kinetika i Kataliz, 21 (6), 1390 (1980).

25. W.R. Seeker, M.S. Thesis, Kansas State University, 1976.

26. W.R. Seeker, T.W. Lester, and J.F. Merklin, Rev. Sci. Instrum., 51, (11), 1523 (1980).

27. S.N. Vaughn, Ph.D. Dissertation, Kansas State Unviersity, 1980.

28. S.L. Szydlowski, M.S. Thesis, Kansas State Unviersity, 1980.

29. A.G. Gaydon an I.R. Hurle, The Shock Tube in High-Temperature Chemical Physics (Reinhold Publishing Corporation, New York, 1963).

30. A.H. Shapiro, The Dynamics and Thermodynamics of Compressible Fluid Flow, Vol. 1 (Ronald Press Company, New York, 1954).

31. E. Tschuikow-Roux, Phys. Fluids, 8 (5), 821 (1965).

32. G. Breipohl, M.S. Thesis, Kansas State University, 1979.

33. W.A. Dietz, Journal of Gas Chromatography, 68, 5 (1967).

34. K.J. Laidler, Chemical Kinetics (McGraw-Hill Book Company, New York, 1965).

35. M.D. Gordon, K.P. Lavroskii, and A.N. Rumyantsev, Dokl. Akad. Nauk SSSR, 191 (6), 1289 (1970).

36. J.D. Bittner an J.B. Howard, in Particulate Carbon: Formation During Combustion, edited by D.C. Siegla and G.W. Smith, General Motors Research Laboratories, 1980, p. 109.

37. S. Sandler and Y. Chung, Ind. Eng. Chem., 53 (5), 391 (1961).

38. S.L.K. Wittig, Phys. Fluids, 12 Supp.I, I-133 (1969).

39. K. Fritz and H. Gronig, in Shock Tube and Shock Wave Research, edited by B. Ahlborn, A. Hertzberg, and D. Russell (University of Washington Press, Seattle, 1977), p. 383.

40. I.B. Kennedy and A.M. Neville, Basic Statistics Methods for Engineers and Scientists (IEP A Dun-Donnelly, New York, 1976).

APPENDIX A

Correction for Finite Rate Cooling

A feature of the single pulse shock tube which must be taken into consideration when determining the kinetics of reactions is the finite cooling rate. Though the cooling rate is up to -5×10^5 K/sec, depending upon the diluent gas composition, reactions with low activation energies (E_a < kcal/mole) will continue to occur during the cooling phase. The additional products which are formed during the cooling of the gases by the rarefaction fan must be taken into account if useful kinetic data are to be acquired. A correction factor to compensate for the finite cooling has been given by Tschuikow-Roux,[31] and is briefly explained below.

The cooling of gases behind the reflected shock front is an isentropic process, for which the relationship between pressure and temperature is

$$\left(\frac{P(t)}{P_5}\right)^{\frac{\gamma-1}{\gamma}} = \frac{T(t)}{T}. \qquad (A.1)$$

From this equation, the finite cooling rate may be determined to be

$$m = \left(\frac{dT}{dt}\right) = \left(\frac{\gamma-1}{\gamma}\right) \frac{T_5}{P_5} \left(\frac{dP}{dt}\right) \qquad (A.2)$$

where (dP/dt) is measured from the pressure history of the experimental gases (see Fig. 2.4). Figure A.1 shows an idealized pressure trace for reference. In argon, this cooling rate is approximately -5×10^5 K/sec.

If the temperature at time t is defined as

$$T(t) = T_5 + \frac{dT}{dt} (t - t), \qquad (A.3)$$

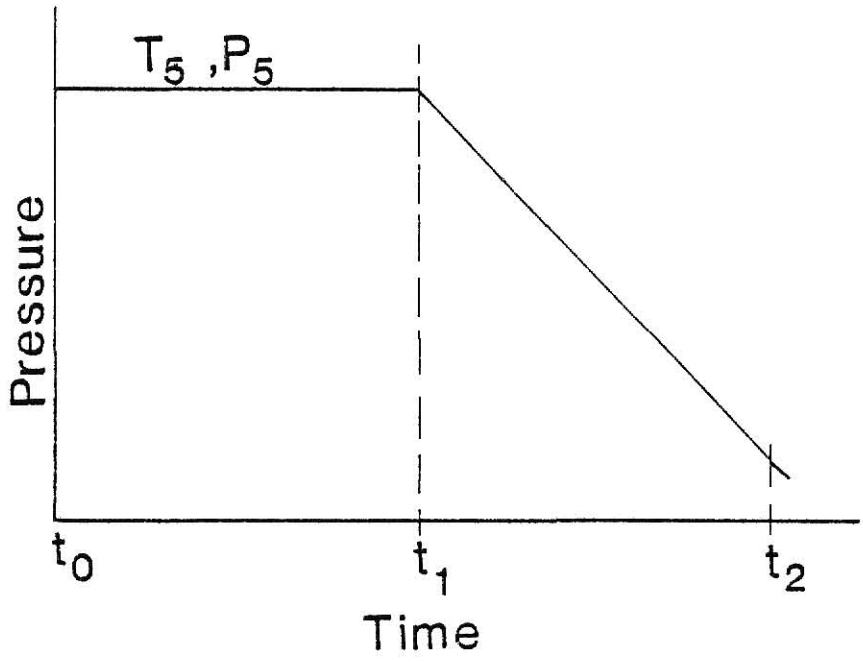

Fig. A.1 Idealized pressure history

with t_1 being the time at the start of the cooling process, and

$$\Delta T = T_5 - T(t), \tag{A.4}$$

then the following equation may be written,

$$\frac{\Delta T}{T_5} = \frac{-m}{T_5}(t - t_1). \tag{A.5}$$

Also, the approximation

$$\frac{1}{T(t)} = (1 + \frac{\Delta T}{T_5})/T_5 \tag{A.6}$$

can be made if $\Delta T < T_5$. Assuming that the amount of reactant N present at time T_2 corresponds to a rate constant which has decreased to 10^{-2} of the value of the constant during the nominal dwell time for the gases behind the reflected shock, Eq. A.3 may be defined as

$$\begin{aligned} \Delta T' &= T_5 - T(t_2) \\ &= \frac{2T_5^2}{2T_5 + E_a/R\ell n10}, \end{aligned} \tag{A.7}$$

where E_a is the activation energy and R, the universal gas constant. Assuming a first order reaction for reactant N,

$$\begin{aligned} \ell n \frac{N(t_2)}{N(t_1)} = K_c \Delta t' &= A\int_{t_1}^{t_2} \exp\{\frac{-E_a}{R}[\frac{1}{T_5} - \frac{1}{T(t)}]dt \\ &= A\int_{t_1}^{t_2} \exp\{\frac{-E_a}{RT_5}[1 - \frac{m}{T_5}(t - t_1)]dt \\ &= -A\frac{T}{E_a}\frac{T_5^2}{m} e^{-E/RT_5}[1 - e^{-E\Delta T'/RT_5^2}] \end{aligned} \tag{A.8}$$

where k_c is the true rate constant at T_5 defined as

$$k_c = A \exp(-E_a/RT_5). \tag{A.9}$$

The correction to the dwell time, t_1, is $\Delta T'$.

From the analysis of products, $N(t_2)$ is known, and an uncorrected rate constant, k_{uc}, is determined. The corrected rate constant, k_c, can then be determined by

$$\ln \frac{N(t_2)}{N(t_0)} = \ln \frac{N(t_1)}{N(t_0)} - \ln \frac{N(t_1)}{N(t_2)} \tag{A.10}$$

or

$$k_{uc}t_1 = k_c t_1 - k_c \Delta t'. \tag{A.11}$$

Thus, the corrected rate constant is

$$k_c = \frac{k_{uc}}{[1 \oplus \Delta t'/t_1]}. \tag{A.12}$$

Figure A.2 is a plot of $\Delta t'$ as a function of reaction temperature for varying activation energies. To find the $\Delta t'$, an estimate of the activation energy must be made, a new activation energy calculated, and iterations carried out until convergence occurs. The number of iterations necessary depends upon the initial guess for the activation energy, although convergence is usually achieved within only a few calculations.

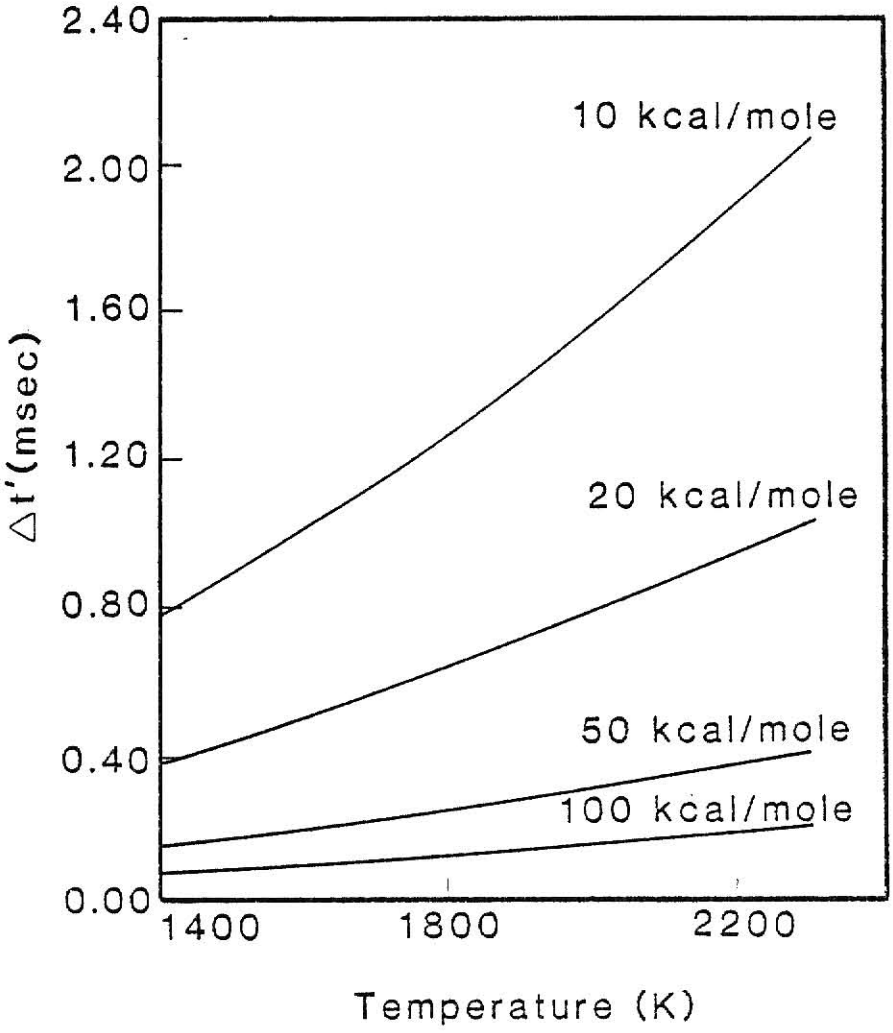

Fig. A.2 Finite cooling rate correction as a function of reaction temperature for specified activation energies

APPENDIX B

Validation of Temperature Measurements

To insure the accuracy of the reaction temperature, T_5, based on the gas dynamics of a single pulse shock tube, experiments were conducted with a relatively well characterized reaction system. The pyrolysis of n-butane was studied over a temperature range of 1185-1417 K using 0.2 mol% n-butane in argon. Comparison of the experimental first order rate constant to the values found in the literature revealed that reaction temperatures based on measurement of the shock speed by the pressure transducers, mounted as described in Section 2.1, needed no correction.

Experimental

N-butane (Matheson, Instrument grade) was diluted with argon (99.995% purity) to yield a mixture with approximately 0.2 mol% n-butane. With the in-line ball valve closed (see Fig. 2.2), the test section of the SPST was filled with the n-butane/argon mixture to a predetermined pressure. The low pressure section of the tube was pressurized to the same pressure using argon. The driver section was then filled with helium (99.99% purity). The in-line ball valve was opened, the shock initiated, and the valve immediately closed. Sampling of the gaseous mixture in the experimental section was done, using a 75 cm^3 stainless steel container, one hour after the shock was completed. The sample was then analyzed on a Tracor Model 560 gas chromatograph with a column packed with 10% SP-2250 on 100/120 Supelcoport (Supelco). The peak area of the n-butane in the sample was compared to the peak area of n-butane in the original mixture. Other experimental procedures were as described in Chapter 2.

Results

Data from the n-butane pyrolysis experiments are listed in Table B.1. The reaction rate constant for each temperature was calculated for a first order reaction with finite cooling rate correction.[31] The rate constants were also calculated for a reaction order of 3/2. However, based on a least squares fit, the data best fit a reaction order of one, with the rate constant being

$$k_1(sec^{-1}) = (2.4 \times 10^9) \exp(-21,930/T) \qquad (B.1)$$

The activation energy is 43.6 kcal/mole.

Table B.2 lists the rate orders and activation energies for the thermal decomposition of n-butane as reported in the literature. The rate constant obtained in the present study falls within the range of values found by other researchers. The discrepancies in the values reported for the activation energy may be partly attributed to the different methods used to study the n-butane system. Especially in flow reactors, there exists a greater possibility of reactions being influenced by the reactor surface and of the existence of temperature gradients which lead to the possible overestimation of the activation energy.

Table B.1. Results for the pyrolysis of n-butane.

Shock	T_5 (K)	t_{dw} (msec)	$\frac{[C_4H_{10}]}{[C_4H_{10}]_0}$	ln k_1 (sec^{-1})
3-30-4	1301	1.2	0.813	5.204
3-30-7b	1236	0.7	0.967	3.700
3-30-8b	1249	1.0	0.929	4.165
3-30-3	1212	1.0	0.976	3.055
3-31-8b	1417	1.1	0.334	6.754
4-1-7b	1295	1.1	0.948	3.753
4-1-9b	1285	1.0	0.959	3.585
4-4-4	1185	0.9	0.931	4.246
4-4-3	1370	1.0	0.692	5.752

Table B.2. Rate constants and activation energies for the decomposition of n-butane

Investigators	Method	Temperature Range K	Reaction Order	Frequency Factor	E_a (kcal/mole)
Sandler and Chung[37]	Flow reactor annular	638- 696	1	9.6×10^9	45.6
	tubular	628- 701	1	2.65×10^9	44.6
Wittig[38]	Shock tube	900-1500	1	3.22×10^9	41.7
Fritz and Gronig[39]	Shock tube	1170-1570	3/2	5.9×10^{12}	38.4
Vaughn[27]	Shock tube	1000-1430	1	3.8×10^9	42.8

APPENDIX C

Error Analysis

Errors in the values of parameters were determined in two manners. If the parameter was measured directly through the use of an instrument or gauge, the error in the measurement was determined by the precision of the system. For example, the error in the measurement of the pressure was one half of a division on the pressure gauge. If the value was calculated from an equation, the error was considered to be the standard deviation, which is defined by [40]

$$\sigma_A^2 = \left(\frac{\partial A}{\partial x}\right)^2 \sigma_x^2 + \left(\frac{\partial A}{\partial y}\right)^2 \sigma_y^2 + \left(\frac{\partial A}{\partial z}\right)^2 \sigma_z^2 + \ldots \qquad (C.1)$$

Table C.1 lists the errors of parameters used in this study. It should be noted that these error values include the worst cases encountered in the measurements.

The systematic error in the sampling system and procedure was evaluated through two experiments using 36 mol% argon/64 mol% hydrogen as the experimental gas. Table C.2 lists the data from these experiments. The first experiment consisted of filling the low pressure and test sections with the experimental gases to a pressure characteristic of the equilibrium pressure of the tube after an experiment. Sampling was then carried out as described in Section 2.1. The second experiment included the complete procedure for the initiation of a shock in the tube. Two samples were acquired, one from the dump bottle and the other from the usual sample bottle. Analysis of these samples led to the conclusion that the systematic error of the sampling procedure was on the order of 1%.

Table C.1. Values obtained from error analysis

Parameter	Error measured	Error calculated
Dwell time, t_{dw}	±0.1 msec	
Mach of incident shock, M_1		±0.02
Initial temperature, T_1	±3 K	
Initial pressure, P_1	±10 Torr	
Reaction temperature, T_5		±25 K
Equilibrium pressure, P_e	±4 Pa	
Area of peaks, A_a, A_i	±3% of area	
Stock mixture concentration, C_o		±0.001
Product yield, yi		±6% yield
Activation energy, E_a		±0.6 kcal/mole
Mass fractional yield		±10% yield

Table C.2. Data from experiments to determine systematic error of sampling system

Sample	Area of Peak	Standard	Area of Peak	Initial Pressure	Equilibrium Pressure	moles detected / initial moles
1 (36% Argon)	77 X 512 (argon)	100% Argon	100 X 1024	2.8×10^5 Pa	2.8×10^5 Pa	0.35 argon
96 (dump)	32 X 256 (hydrogen)	65% H_2/36% A	66 X 612 (hydrogen)	3.3×10^4 Pa	2.14×10^5 Pa	1.01 (hydrogen)
4	32 X 256 (hydrogen)	64% H_2/36% A	66 X 512 (hydrogen)	3.3×10^4 Pa	2.14×10^5 Pa	1.01 (hydrogen)

PYROLYSIS OF CYCLOHEXANE AND BENZENE/CYCLOHEXANE MIXTURES IN A SINGLE PULSE SHOCK TUBE

by

B. Ellen Johnson

B.S., Kansas State University, 1981

AN ABSTRACT OF A MASTER'S THESIS

submitted in partial fulfillment of the
requirements for the degree

Master of Science

Department of Nuclear Engineering
KANSAS STATE UNIVERSITY
Manhattan, Kansas

1982

ABSTRACT

The pyrolysis of cyclohexane in a single pulse shock tube was investigated for reaction temperatures of 1400-2400 K and reaction pressures of 7-13 X 10^5 Pa. Additional studies were carried out for reactant systems of benzene and benzene/cyclohexane mixtures. The reactant concentrations were approximately 1.3 mol% in argon. Quantitative and qualitative analyses were performed for certain gaseous products of pyrolysis. Liquid and solid products were collected on aluminum liners placed in the shock tube and were gravimetrically analyzed.

The principal products of thermal decomposition of cyclohexane are methane, ethylene, and acetylene. The yield of acetylene increases with reaction temperature, while those of ethylene and methane reach maxima near 1900 K. Propene, propyne, 1,3-butadiene, and 1,2-butadiene were also observed, along with traces of benzene. A mechanism, based on the decomposition of methylcyclopentyl radicals which accounts for the order of appearance of the C_3 and C_4 hydrocarbons, is discussed. Comparison of the gaseous yields of the cyclohexane, benzene, and benzene/cyclohexane mixtures indicates that the aliphatic and aromatic molecules decompose independently. A first order global rate constant, with a frequency factor of 1.2 X 10^5 sec^{-1} and an activation energy of 14.3 kcal/mole, adequately describes the disappearance of cyclohexane in the systems studied. The activation energy for cyclohexane pyrolysis is much lower than that for benzene decomposition, indicative of the stability of the aromatic ring. Gravimetric results of the solid and liquid products reveal that the weight percent yield does not vary with

reactant. However, visual observation of the solid and liquid products indicates that the production of liquids occurs at lower temperatures from cyclohexane than from benzene. The amount of solids present increases with temperature. As the aromatic content of the system increased, the tendency to form particulates increased, and the temperature at which particles were first observed decreased. This supports the view that liquid droplets, composed of polyaromatic hydrocarbons, are precursors in the formatino of soot.